THERMAL PERFORMANCE OF MICROENCAPSULATED PHASE MATERIAL (MPCM) SLURRY IN A COAXIAL HEAT EXCHANGER

A Thesis

by

KUN YU

Submitted to the Office of Graduate and Professional Studies of
Texas A&M University
in partial fulfillment of the requirements for the degree of

MASTER OF SCIENCE

Chair of Committee,	Jorge L. Alvarado
Committee Members,	Michael Pate
	Karen Vierow
Head of Department,	Andreas A. Polycarpou

May 2014

Major Subject: Mechanical Engineering

ABSTRACT

Microencapsulated phase change material (MPCM) slurries and coil heat exchangers had been recently studied separately as enhancers of convective heat transfer processes. Due to the larger apparent heat related to the phase change process of the phase change material (PCM), MPCMs have shown improved heat capacity when compared with water. It has also shown better performance as heat storage and secondary heat transfer fluid. Coil heat exchangers had been already used in industrial applications due to their high heat transfer performance. This study explores the use of MPCM and coil heat exchanger in terms of heat transfer efficiency and pressure drop when these two enhancers work together.

The objective of this study is to understand the effects of microencapsulated phase change material (MPCM) slurries as heat transfer fluid (HTF) on coil heat exchangers. An in depth survey of the literature pertaining to both coil heat exchangers and MPCMs has been conducted in an effort to understand the effect of using MPCMs as HTFs in different heat exchangers. The review covers the basic understanding of heat exchangers under laminar and turbulent flow as well as a more in depth review of helical coil and coaxial heat exchangers and their flow and heat transfer characteristics. Previous research in the field of MPCM's is also presented to help understand the effects of their thermal properties including density, viscosity, thermal conductivity, and specific heat on heat transfer performance. A detailed description of the present experimental setup is given, which includes physical dimensions as well as operating parameters. Steps taken during the data

reduction process are included in order to facilitate the analysis of the results. Experiments were conducted using a fully instrumented heat transfer system under laminar and turbulent flow conditions of MPCM slurry at different flow rates and mass fractions. The results are compared to each other as well as to heat transfer correlations from previous studies. Heat exchanger effectiveness calculations and results are also presented. Using these analyses, conclusions have been made on the effects of using MPCM slurry in coaxial coil heat exchangers. Results show that MPCM flows are characterized by high pressure drop, but higher heat transfer rates at a certain mass fraction. Finally, future research directions are proposed based upon the present results.

ACKNOWLEDGEMENTS

I would like to thank my advisor Dr. Jorge L. Alvarado for his constant guidance, help, and support extended to me during the entire duration of the research project. His constant encouragement and patient approach helped me complete this project successfully. I would like to thank him for giving me the opportunity to do this research project.

I would like to thank Dr. Wilson Terrell for his help and guidance, particularly during the initial stages of the project. I have learned a lot of things from him and he have been a great source of inspiration to me. I would like to thank my committee members, Dr. Michael Pate, and Dr. Karen Vierow for their support and co-operation during the course of this project. They gave me very valuable input during the experimental and analysis stages of the project.

I would like to thank my lab mate Minsuk Kong. He helped with the design and construction of the heat transfer system required for the successful completion of the project. I would like to thank him for his valuable time and help provided during the course of experiments.

I would like to thank all my colleagues and friends who have helped me and supported me. Finally, I would like to thank my parents for their love and constant encouragement.

TABLE OF CONTENTS

Page

LIST OF FIGURES

Page

LIST OF TABLES

Page

1. INTRODUCTION

With the development of the human society, energy and environmental issues have gained more and more attention because they are intrinsically linked with the survival of the human beings. Possible solutions to the energy issue may include using renewable energy and waste heat, improving the energy efficiency, to name a few options. Furthermore refrigeration and air conditioning is one of the heavy energy consumers, many HVAC systems rely heavily on water-based heat transfer fluids; however, water has become a scare commodity in many parts of the world.

One approach to reduce the amount of water-based heat transfer fluids used is to incorporate phase change materials into the HTF. Phase change materials (PCM) used in secondary refrigeration loops allows for a significant reduction in the use of water and provide an increase in energy storage capacity. It is very important to select the appropriate working fluid for the secondary refrigeration loop in the operation and cost of HVAC systems.

Recently, more studies have focused on the use of microencapsulated phase change material slurries (MPCM), which can potentially be used in the secondary refrigeration and air conditioning systems. The main benefits of MPCMs over other heat transfer fluids, such as ice slurry, in industrial applications are as follows: (1) the phase change temperature range of PCM can be adjusted for air conditioning system by properly selecting PCM without having to produce and store ice-water slurries needed for air conditioning; (2) the MPCM's typical particle size is smaller than that of ice slurry, which

minimizes the risk of clogging in pipes; and (3) the energy efficiency when using MPCM for the refrigerating system could be higher than using ice slurry because they HVAC systems do not have to operate at low temperatures.

Research has shown that coil heat exchangers (CHXs) depict higher heat transfer enhancement due to their unique design. These works have also validated the benefits of the CHXs when using mainly water as heat transfer, but none of the studies have considered the use of MPCM slurries and CHXs together. This current study includes heat transfer results of MPCM in coaxial coil heat exchangers, which clearly show the effects of using MPCM slurries in a heat transfer system.

2. LITERATURE REVIEW

2.1 MPCM

In the past 25 years, engineers and researchers have begun to introduce new materials and fluids into heat exchangers in hopes of increasing heat transfer performance. Materials that change phases within the operational temperatures of the heat exchangers were studied in order to utilize the added heat capacity from the latent heat of melting of the material. When introduced into the heat exchanger fluid, the new material is shown to increase heat capacity with the same or less temperature difference as before. However, without somehow avoiding the separation or precipitation of the phase change material from the working fluid during the solidification process, the phase change material tended to agglomerate and create obstructions in heat exchangers. To prevent this, microencapsulated phase change materials (MPCMs) were introduced. The idea behind this was to prevent agglomeration while still obtaining increased specific heat of the working fluid during the phase change process. A considerable number of studies have been conducted in the last 15 years in order to better understand the processes by which the introduction of MPCMs affects heat transfer.

In 1999, Y. Yamagishi [1] conducted an in-depth study on the flow and heat transfer characteristics of an MPCM slurry under constant heat flux. The phase change material (PCM) used was Octadecane, which has a latent heat of 223 kJ/kg. The particles had an average diameter of 6.3 μm. It was assumed the average capsule thickness was 0.1 μm. The particles were mixed with water at five different varying volume fractions from

0.07 to 0.30. As shown in previous study, microencapsulating a PCM causes some degree of supercooling, the difference in temperature between the melting and solidification temperature. The solidification temperature of MPCM's will be somewhat lower than the melting temperature, and is detrimental to the heat transfer process. The amount of supercooling was reduced from 13 K to 5 K by the introduction of a dispersing agent into the phase change material before the encapsulisation process. Heat transfer tests with MPCM/water were compared to tests with water using a well calibrated heat transfer loop. The MPCM slurry was tested in the loop with zero heat flux to provide insight on the rheological properties of the fluid. The results show the MPCM slurry acts as a Newtonian fluid, with a transition from laminar to turbulent regime around a Reynolds number of 2300, which is normal for circular pipe flow. It was also seen the pressure drop for increasing MPCM volume fraction increased for the same mean flow velocity due to the increased slurry viscosity. From this information it was found that there is a nonlinear relationship on viscosity versus particle volume fraction. In almost all the cases, the temperature of the flow has three distinct regions similar to the Figure 1. Regions I and III corresponded to a temperature increase due to the sensible heat of the slurry, while Region II begins at the point of MPCM melting temperature. This temperature theoretically remains constant until all the particles have melted where it once again begins to increase in temperature due to the thermal energy gain from sensible heat. With a lower heat flux, Region II becomes larger, not allowing the particles to completely melt before the end of the test section. The experimental results slightly deviate from the calculated results of

Figure 1 due to the supercooling phenomenon as well as the finite melting rates of the particles.

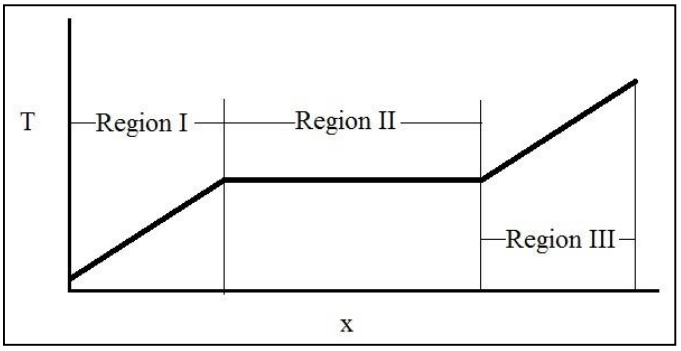

Figure 1 Temperature vs. axial distance for a MPCM slurry under constant heat flux

When comparing the local heat transfer coefficients of water versus MPCM slurry for the same flowrate, at the beginning and the end of the test section the MPCM is seen to have a markedly lower heat transfer coefficient being due to the increased slurry viscosity. In Regions I and II however, an increase in heat transfer coefficient is seen, with a maximum slightly under the heat transfer coefficient of water. The increase in heat transfer coefficient could be caused by the melting of the MPCM particles; thus increasing the effective specific heat of the slurry. After the particles have melted, a drop is seen in the heat transfer coefficient towards what is predicted by heat transfer to a single-phase fluid. The heat transfer coefficient results also showed that for a larger input heat flux, a lower maximum heat transfer coefficient was achieved, which is thought to be caused by

the increasing thickness of the thermal boundary layer, causing the particles in the turbulent core to melt before reaching the tube wall [1]. When comparing heat transfer coefficients for different particle volume fractions under the same inlet temperatures, heat flux, and Reynolds numbers, the larger particle volume fraction resulted in a larger maximum heat transfer coefficient. However for the same flowrate, a lower volume fraction was seen to have a higher local heat transfer coefficient. This was said to be due to the decrease in turbulence (lower Reynolds number) from the increase in the slurry viscosity, where the lower turbulence did not allow as many particles from the core to travel towards the tube wall. What this means is that higher volume particle fractions will not always result in a higher heat transfer coefficient, as there are competing effects between higher slurry viscosity and a higher effective specific heat. At relatively high mass fractions, a laminarization of the flow was seen to occur, drastically decreasing the local heat transfer coefficients. It was postulated that due to the laminar flow, a layer of fully melted particles forms along the tube wall while the core region is filled with solid particles. It was concluded that for the same particle volume fraction, turbulent flow is more effective than laminar flow, even when the slurry undergoes phase change. In light of all the presented results, it was seen that for the same flowrate in the turbulent flow regime, the local heat transfer coefficient of the MPCM slurry was always lower than that of pure water.

In 2002, Hu and Zhang [2] produced a numerical study on laminar heat transfer of MPCMs in a circular pipe under constant heat flux. The study looked at the thermally developing region as well as the fully developed region. Since the variability of specific

heat throughout the melting temperature range of the MPCM is not well known, 4 different functions were looked at and were shown to effect the Nusselt number through the thermal entry region but were shown to converge at large axial distances. The fluid was assumed to have a Newtonian behavior up to a volumetric concentration of 0.25. A sensitivity analysis was conducted to study the effects of the Stefan number, degree of subcooling, melting temperature range, particle diameter, and volumetric concentration on the heat transfer enhancement. Since volumetric concentration affects both the effective thermal conductivity as well as the mean heat transfer coefficient, it was seen to have the largest effect on heat transfer. Based upon the results, a low degree of subcooling, a small melting temperature range, and a large particle diameter were seen to benefit heat transfer the most, but individually not as much as volumetric concentration. As with any other single-phase flow, an increase in Reynolds number was shown to increase the Nusselt number.

In 2007, J. L. Alvarado et al. [3] conducted a study on MPCM heat transfer and pressure drop using a set of heat transfer sections under constant heat flux. The study also included analysis of the MPCM construction and efforts to reduce the effect of supercooling. The PCM used was Tetradecane with an average size of 2-10 μm. Tetradecanol was used as a nucleating agent to reduce supercooling. Viscosity analysis showed behavior reminiscent of a Newtonian fluid up to mass concentrations of 17.7%. The pressure drop results did not indicate any significant increase in pumping power. The apparent specific heat used in heat transfer analysis was calculated as a function of mass fraction. All results were within the Reynolds range of 3900-7500. Under the same flow conditions, an increase in heat capacity of 40% was seen for 7% mass fraction slurry.

Under the same conditions, the heat transfer coefficient was seen to vary along the pipe, reaching a maximum near the melting point of the MPCM. Regardless, at the same flow velocities, a lower heat transfer coefficient was seen for the slurry due to reduced momentum transfer.

In 2008, B. Chen et al. [4] studied heat transfer of MPCM slurry under laminar flow through a circular pipe. The pipe was stainless steel and a constant heat flux boundary condition was applied through Joule Heating by using the pipe as a resistance. The PCM used was 1-bromohexadecane with a melting temperature around 15 ℃. Density and specific heat of the MPCM were calculated based upon the mean of its solid and liquid properties. The thermal conductivity of the particle was calculated by estimating its thermal resistance. The slurry density and specific heat were calculated based upon the mass fraction. In the region of phase change, the specific heat was taken to be a function of the heat of fusion. The slurry thermal conductivity was calculated using Maxwell's relation. The viscosity of the slurry was shown to be Newtonian for all specimens, up to a 15.8% weight fraction. The effective specific heat of the slurry was seen to increase up to 28.1% relative to water during the phase change process. An applicable pump power analysis was performed to determine the decrease in consumption through using MPCM slurry versus water. Due to the higher heat capacity, a decrease of 67.5% in pump work can be seen while removing 750W using the 15.8% weight fraction MPCM slurry. In 2009, R. Zeng et al. [5] used this same experimental data and compared it to a numerical simulation based upon an enthalpy model. It should be noted that in the phase change region, a sine curve was chosen to represent the changing value of specific heat of the

slurry. The Nusselt number along the pipe is shown to reach a maximum at the onset of the melting region and a minimum at the end of the melting region, these values being higher and lower than the numerical results for water, respectively. The Stefan number, seen in Equation (1), as well as the phase change temperature range were shown to effect the Nusselt number the most, while the effects of particle diameter, Reynolds number, and particle concentration were shown to cause smaller effects.

$$Ste = \frac{C_p \cdot \Delta T_{fus}}{\lambda} \tag{1}$$

In 2010, Taherian [6] presented model analysis of the effects of using a blend of MPCMs and nanofluids in water on heat transfer. The idea behind this is to combine the high effective specific heats of MPCM's with the high thermal conductivity of a nanofluid to produce a better heat transfer fluid than would be seen using the individual constituents. In a simulated counter flow concentric tube heat exchanger, the effects of the percentage of MPCM's that undergo phase change as well as the amount of nanofluids present in the blend were analyzed. The effective specific heat was shown to be large for a high phase change percentage combined with a small mass fraction of nanofluids. At higher nanofluid mass fractions, the effective specific heat converges towards a single value, regardless of the percent of phase change.

In 2010, Nakagawa et al. [7] conducted an experimental study using MPCMs through a circular mini pipe. The PCM used was lauric acid with a melting temperature of about 45°C. The average size of the particle was 3.27 μm and the particle mass concentration was varied from 0 to 5%. Flourinated dielectric fluid was used as the working fluid. The specific heat of the slurry is calculated based upon the single-phase

properties and the mass fractions of the fluid and particles. The effect of latent heat was taken into account when total heat transport rate was calculated. The results show that with increase in mass concentration produces a decrease in wall temperature rise along the axis. The overall heat transport rate is shown to increase with increasing mass concentration and increasing flowrate. The results for Nusselt number show good correlation with theory when using the dielectric fluid. When using the slurry, the Nusselt number increases towards the end of the test section, with a maximum Nusselt number of around 35 for a mass concentration of 5%. It was assumed that the high Nusselt number values were overestimated due to the assumption of a bulk fluid linear temperature profile along the axis. Because of the melting process, the temperature of the slurry will vary along the length of the tube, and a linear temperature relationship is not accurate.

As the recent studies show, little to nothing has been done in the field of MPCM as HTF in coil heat exchangers (CHE). This study is a first attempt to understand how MCPMs perform in CHE.

Mulligan et al. [8] conducted a series of experiments of microencapsulated slurries with both water and silicone oil as base fluids. The kinds of phase change materials which were studied are n-octadecane, n-heptadecane, n-eicosane and n-nonadecane. The sizes of these PCMs varied between 10 and 30 μm. The capsules were made of 83% core material and 17% wall material. Polymer material was used to make the wall with phase separation techniques. Every kind of phase change material had its own optimum operating condition where maximum phase change was observed. This depended on the melting point of the MPCMs, flow rates and heating. The full improvement was seen only

at concentrations 25% or above even if effective specific heat improved with a small amount of PCM. Heat transfer coefficients improved significantly for higher concentrations but less at lower concentrations.

2.2 Coil heat exchanger

Coil heat exchangers are routinely used in industrial applications because they can provide a substantial amount of heat transfer in small configuration. Most coil heat exchangers consist of concentric tubes where heat is allowed to flow from one tube to the other. This allows for more heat transfer surface area in a smaller configuration but usually leads to higher pressure drop across the heat exchanger.

The Dean number, an important parameter for helical coils, is defined as shown in Equation (2). Dean number represents the ratio of the viscous force acting on a fluid flowing in a curved pipe to the centrifugal force. The Dean number will never be larger than the Reynolds number for the same flow.

$$De = \frac{\rho V d}{\mu}\sqrt{\frac{d}{D}} = Re\sqrt{\frac{d}{D}} \tag{2}$$

In 1963, Seban and McLaughlin [9] studied heat transfer through a helical coil using two different curvature diameter ratios, d/D, of 0.0588 and 0.0096. The curvature diameter ratio is defined as the ratio of the inner diameter of the pipe, d, to the curvature diameter of the helix, D. The flow was varied from laminar to turbulent for a range of $12 < Re < 65{,}000$. Heat was applied to the coil through the use of an AC current along the length of the stainless steel coil. This provided for an almost constant heat flux boundary condition and is known as Joule Heating. The experimental set up consisted of multiple

coils with multiple thermocouples on each coil. It was noted that even though circumferential conduction of heat was neglected, due to the nature of the flow in a helical coil, the heat transfer coefficients at the inside and outside halves of the pipe were substantially different in the laminar flow regime. Pressure taps were also included on each end of the coil bank. The local heat transfer coefficients for laminar flow were found to be consistently larger on the outer half (peripherally) than on the inner half. For all cases, a larger heat transfer coefficient was seen relative to a straight tube. There was also evidence to support a shorter entry length region, resulting in a shorter distance before asymptotic heat transfer values were reached. The asymptotic value was shown to be a function of $RePr^{0.3}$, and was not constant as is seen in straight tube flow. In the laminar region, there was no evidence to support a dependency on the curvature diameter ratio, as the heat transfer coefficients for the large and small coils were similar. An empirical best fit of the data was given in the form of Equation (3) based upon the asymptotic heat transfer coefficients, where A and B are found based upon a curve fit.

$$Nu = A \cdot Re^{B} Pr^{1/3} \tag{3}$$

$$\frac{f}{8} = \frac{Nu}{Re \cdot Pr} Pr^{2/3} \tag{4}$$

Due to the similarity of this equation to the Dittus-Boelter correlation, it was assumed that these heat transfer coefficients could be related to the friction factor in a way similar to the Chilton-Colburn analogy as seen in Equation (4).

In 1971, Dravid [10] conducted a numerical and experimental study on heat transfer through coils. The research was restricted to the laminar regime but for *De* > 100.

The numerical results were based upon helical coils with small curvature diameter ratios and fully developed velocity fields. The numerical results showed that due to the complex flow field, large cyclical oscillations in axial wall temperature occur with the oscillations being damped at larger axial distances. Their experimental setup consisted of thick copper tubing helically wrapped in a Teflon coated Nichrome wire. This was then formed into a helix with a curvature diameter of 137 mm (5.4 in). creating an overall curvature diameter ratio, d/D = 0.0536. It should be noted here that many studies refer ambiguously to curvature diameter ratio, and unless otherwise noted, it should be thought of as d/D. Water was used as the working fluid. The experimental results matched very well with the numerical results, both showing damped oscillatory motion. The short entry length region relative to a straight tube was also seen in the experiment. In 1974, Kalb and Seader [11] produced a numerical study on helical coiled tubes for Dean numbers up to 1200. The boundary condition was chosen to be constant axial surface temperature, as at the time it was the least studied condition, as well as it having more applicability to real world scenarios. Based upon their analysis, the fully developed temperature field was shown to change markedly with increasing Prandtl number. It was also shown that the thermal boundary condition plays a role in fully developed temperature profiles, with a uniform wall temperature boundary condition contributing to a wider range of temperatures from the wall to the core of the flow field. It was also shown that for middle range Prandtl numbers of 0.7 to 5, the boundary condition of uniform wall temperature provides for a Nusselt number with a smaller dependence on Prandtl number when compared with uniform axial heat flux boundary condition. Kalb and Seader proposed Equation (5) as a

helical coil heat transfer correlation, valid for 0.7 < Pr < 5, 80 < De < 1200 and 0.01 < d/D < 0.1.

$$Nu = 0.836De^{0.5}Pr^{0.1} \tag{5}$$

In 1978, Janssen and Hoogendoorn [12] produced a numerical and experimental study that was focused on Prandtl numbers from 10 to 500. The experimental setup consisted of helically coiled stainless steel tubes and Joule Heating was used to produce an axially uniform heat flux boundary condition. The experiment also considered a constant surface temperature boundary condition by placing the coil in a shell with condensed steam. The numerical results showed the same damped cyclical nature of the Nusselt number as seen from Dravid [10]. It was also seen that for *De* < 20, the asymptotic Nusselt number was correlated with De^2Pr. The proposed correlation as seen in Equation (6) is valid for *De* < 20 and $\left(De^2Pr\right)^{1/2} > 1\ x\ 10^2$. The experimental results showed that for *De* > 20, the Nusselt number had little dependence on *d/D* and was proportional to $Pr^{1/6}$, which is unlike the previous studies. The results also showed little difference between the Nusselt numbers from the different boundary conditions, which was mostly assumed to be due to the low temperature dependent viscosity of the fluid in the experiments. Janssen and Hoogendoorn also proposed the correlation seen in Equation (7), valid for $1\ x\ 10^2 < De < 8.3\ x\ 10^2$.

$$Nu = 1.7(De^2Pr)^{1/6} \tag{6}$$

$$Nu = 0.7Re^{0.43}Pr^{1/6}(d/D)^{0.07} \tag{7}$$

In 1981, Manlapaz and Churchill [13] conducted a review of all of the previous experimental and numerical results involving heat transfer in coiled tubes. Their goal was to produce a general correlation for all the different regimes covering 0 < De < 2000 and 0 < Pr < 1600. There were also efforts to include the effects of finite pitch into the correlation. This was done by replacing the Dean number with the Helical number as seen in Equation (8).

$$He = De/[1 + (b/\pi D)^2]^{1/2} \tag{8}$$

In 1989, Prasad et al. [14] conducted an experiment on a coiled tube in a shell, which was one of the first recent experiments on a helically coiled tube in shell heat exchanger. The experimental setup consisted of copper helical coils with diameter ratios D/d of 17.24 and 34.90 for two separate tests. The coils were placed in a large shell. The working fluids used were hot water and air for the coil and shell sides, respectively. The experiments measured both pressure drop and temperature along the coil and shell. The experiments were conducted throughout the laminar and turbulent regime for 1780 < Re < 59,500. The transition from laminar to turbulent regime was determined by the critical Reynolds correlation developed by Ito [15] and used by Seban and McLaughlin [9], as seen in Equation (9). The correlation proposed for the laminar regime is of the same form as Seban and McLaughlin (1963) as seen in Equation (3), but in this case A = 0.25 for 200 < De < 500. A new correlation for the turbulent regime was not proposed, but rather it is said to correlate well with Equation (4) from Seban and McLaughlin (1963). Prasad also proposed shell side correlations similar to the form of the Dittus-Boelter correlation for flow in a circular annulus as seen in Equation (10), where C is a function of D/d ratio. The

variable, C, was found to be 0.057 and 0.110 for D/d = 17.24 and 34.90, respectively. Equation (10) is valid for 30,000 < ReDh < 200,000.

$$Re_{Cr} = 2\ x\ 10^4 \left(\frac{d}{D}\right)^{0.32} \tag{9}$$

$$Nu_s = C \cdot {Re_{Dh}}^{0.8} \tag{10}$$

A 2005 study by T. J. Rennie [16] focused on an experimental study of a helical pipe in pipe heat exchanger. The idea was to reduce the possible zones of dead or no flow in a coil in shell heat exchanger by creating 2 helical pipes, one inside of another. The experimental setup consisted of only 1 turn of a coil with zero pitch so the applicability of the results is somewhat questionable. A large and a small inner coil were tested with the same outer annulus. Regardless, the only measurements taken were of the inlet and outlet temperatures of the inner tube and outer annulus. This was done to not affect the flow field. In order to calculate inner and outer heat transfer coefficients, the Wilson Plot method was used. This method uses the inlet and outlet temperatures and the calculated overall heat transfer coefficient to calculate inner and outer heat transfer coefficients. There is also the assumption that by keeping the mass flow rate of the inner tube constant, it can be assumed that the inner heat transfer coefficient is constant. This method is described in detail by Fernandez-Seara [17]. The results for the inner heat transfer coefficient were similar to that of Dravid [10], but due to the increased variability in the results of the smaller inner coil, the Wilson Plot method did not work as well. The results also showed that operating in parallel or counterflow configuration, the overall heat transfer coefficient did not change appreciably.

A 2006 experimental and numerical study by V. Kumar et al. [18] was conducted on a tube in tube helical heat exchanger. Unlike Rennie [16], the setup had 4 coil turns, providing a larger length for the flow to develop. Hot and cold water were used as the working fluids for the inner coil and outer annulus, respectively. The heat exchanger was operated in the counterflow configuration. The inner and outer tube diameters were 25.4 and 50.8 mm, respectively. The outer annulus contained baffles to hold up the inner coil as well as induce more turbulence. Like Rennie [16], the heat transfer coefficients were calculated using the Wilson Plot method. A numerical analysis was also conducted using the same system design and boundary conditions using FLUENT 6.1. The inner Nusselt number experimental results were compared with the numerical results and were seen to deviate by less than 4%. This provides at least some evidence supporting the viability of the Wilson Plot method for future researchers. The values of the inner Nusselt number reported are slightly higher than the correlations of Kalb and Seader [11] and Manlapaz and Churchill [13] but follow the same trend. The discrepancy was most likely due to the change in boundary conditions. The outer Nusselt number experimental and numerical results deviate 8-10% from each other, and are seen to be 2-3 times higher than straight tube flow.

In 2007, Naphon [19] conducted a study on a complex heat exchanger involving two helical coil banks with fins attached to the coils, inside of a sectioned shell. The heat exchanger was operated in the counter flow configuration. Hot water and cold water were used for the coil and shell sides, respectively. Though no results were presented on inner or outer heat transfer coefficients, results were given relating the heat exchanger effectiveness versus shell and coil flowrates. For low hot water mass flowrates, the heat exchanger effectiveness was seen to increase with increasing coil hot water inlet temperature. At higher hot water flowrates, the effectiveness converges onto a single value, regardless of hot water inlet temperature. The highest effectiveness is seen with the largest shell side flowrate and the lowest coil side flowrate, and the lowest effectiveness is seen when the inverse situation occurs.

3. THESIS OBJECTIVES AND PROPOSED APPROACH

The principal objective of this research work was to determine the effect of industrial formulated MPCM slurries at low mass fraction on the effectiveness and pressure drop of a coiled heat exchanger (CHX) under turbulent flow conditions. A complete characterization of the MPCM slurries was undertaken in order to obtain the key properties needed for the analysis of MPCM in CHX. The results for water-water tests and the water-MPCM tests were compared to determine if the MPCM slurries can substantially improve the heat transfer performance of CHX in laboratory setting. Also, for the analysis part, a code using Engineering Equation Solver (EES) was devedloped to evaluate the performance of the CHX when MPCMs were used.

There are several sub-tasks that needed to be completed in order to accomplish these objectives. These objectives are summarized below.

3.1 Experimental work

A heat transfer loop was designed and assembled at the DXP Pump laboratory in the Thomson Hall building of Texas A&M University. The loop which consisted of two CHX was calibrated under thermal isolation conditions using water to ensure accurate results with heat transfer fluids. Viscosity, density and mass fractions measurements of MPCM slurries have been conducted to understand the physical properties of MPCM. Viscosity measurements were conducted at different temperatures and shear rates using a Brookfield rotary viscometer. Thermal test with water (water-water) as well as with MPCM (water-MPCM) of two mass fraction were conducted as well. These three tests

were conducted under seven different flow rates while keeping inlet and outlet temperatures of the fluid almost constant.

3.2 Analysis work

Once all the heat transfer experiments were conducted, the percentage of MPCM that underwent phase change process was determined in order to make sure the experimental results were valid and comprehensive. Then, the heat rate inputs for the cold and hot sides were calculated, and the differences were compared to make sure heat losses were insignificant. The flow rates and pressure drops of the pump and the system were converted and recorded for analysis too. A code for calculating all the parameters was developed using EES software. The Reynolds number, Dean number, fraction factor, UA, NTU and heat exchanger effectiveness were calculated and compared between water-water tests and water-MPCM tests.

4. EXPERIMENTAL PLAN

4.1 Description of experimental system

The test system consists of two industrial-type coil heat exchangers (CHXs), two pumps, a chiller, a heater tank, two flow meters, one pressure transducer, one multimeter, eight type-T thermocouples, pipes, fittings, clamps and other connecting parts, branches, valves and insulation materials. A full description of each component is provided below.

4.1.1 Coaxial heat exchangers

The coaxial coil heat exchangers employed for this project are two model BTSSC-36 (C-5341-05) manufactured by Turbotec. A cross section view of the coaxial heat exchanger can be seen in Fig 2 and the relevant properties of these CHXs can be found in Table 1.

Figure 2 Cut cross section view of coaxial heat exchanger

Table 1 CHX properties

Property	Property Variable	Value
Curvature diameter of CHX		36.83 cm
Walls thickness		0.1118 cm
Outer core diameter		2.446 cm
Inside core diameter		2.2223 cm
Outer shell diameter		3.81 cm
Inside shell diameter		3.586 cm
Hydraulic diameter of core		2.334 cm
Hydraulic diameter of shell		1.364 cm
Core volume	$Vol_{hx,core}$	0.0018 m^3
Core cross sectional area		4.279 cm^2
Shell cross sectional area		6.462 cm^2
Heat transfer surface length	$L_{hx,core}$	4.206 m
Heat transfer surface area	A_{sur}	0.3084 m^2

4.1.2 Water tank and heater

A reservoir tank equipped with an electric heater manufactured by Tempco was used as the main source of hot water during the experiments. Lines were used to feed the hot water to CHX 1 to be able to heat the fluid to the right temperature. The heating

element came with a temperature controller which was used to control water temperature in thermal loop one.

4.1.3 Pumps and motors

A pump (March TE-5C-MD) circulated the hot heat transfer fluids through the test loop, as shown in Fig 3.The pump which came with its own motor, used to pump hot fluids.

Figure 3 First loop pump

The cold side fluids were pumped using a Goulds Pump with an Emerson C63CXHNY-5070 motor as shown in Fig 4.

Figure 4 Second loop pump

4.1.4 Flow meters

The flow rate of the core side (hot fluid side) in heat exchanger # 2 was controlled using a gate valve and it was measured using an electromagnetic flowmeter model FMG-401 with an accuracy of $\pm 0.5\%$ manufactured by Omega. The full scale of the flowmeter is from 0 to 0.0946 m^3 with an output of 4 to 20 milliamps (mA). It can operate up to temperatures of 120 ℃ and pressures of 2000 kPa (290 Psi). A picture of the style of flowmeter can be seen in Fig 5 which was connected to the data acquisition system. The flowrate for each test was recorded using a computer.

Figure 5 Omega® FMG 400 series flowmeter

The flow rate of the shell side (cold fluid side) in heat exchanger # 2 was controlled using a ball valve and it was measured by a coriolis flowmeter by Endress+Hauser Promass 60M/63M flowmeter (Fig. 6) with an accuracy of $\pm 0.1\%$. This flowmeter can measure mass, density and temperature of different fluids. The full scale of this flowmeter is set from 0 to 31.752 kilograms per minute (kg/min) with an output of 4 to 20 mA.

Figure 6 Endress+Hauser promass 60M/63M flowmeter

4.1.5 Pressure transducer and power supply

A pressure transducer model (Fig 7) 3051 CD4A02A1AH2B1 with an accuracy of up to 0.04% manufactured by Rosemount was used to measure the pressure drop between the inlet and outlet of the HX#2 core. The full scale of these pressure transducers was from 0 to 344.7 ($0 - 50\,psi$) with an output of 4 to 20 mA. The differential pressure sensor measures the input pressure difference to the sensing unit. These devices require a power supply of at least 10.5 volts (VDC) but no more than 55 VDC. For this, it is employed a DC power supply model 382202 manufactured by Extech Instruments.

Figure 7 Pressure transduce by Rosemount

4.1.6 Sample taking station and fluid injection point

A sample taking station was built and connected to the heat transfer loop system to be able to draw fluid samples as needed, as shown in Fig 8. The other section, which consists of a pipe and a valve, was used to add fluids into the loop system.

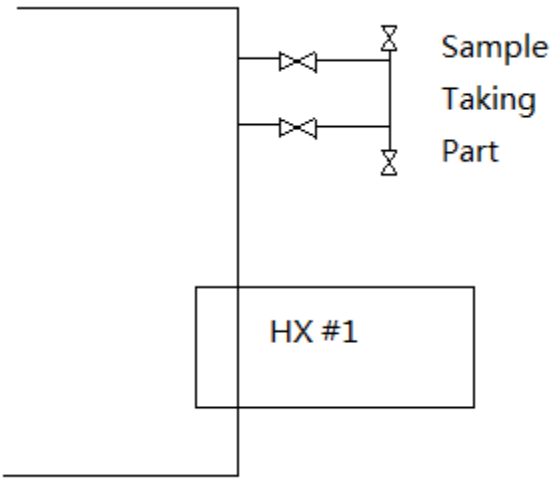

Figure 8 Sample taking part

4.1.7 Water chiller and the bypass valve

The shell side of the heat exchanger #2 (HX#2) was connected by a third loop to the industrial water chiller model SIC-5A manufactured by Shini Plastic Technologies which has already an integrated centrifugal, multi-stage pump of flowrate up to 0.76 L/s (12 GPM) needed in this loop. The chiller consists of one 3.7 kW (5 HP) compressor with a nominal capacity of 4.8 tons. This style of chiller can be seen in Figure 9. The shell side flowrate was recorded for each test off of the readout on the monitor screen of the water chiller. The by-pass valve was used to control the flow of chilled liquid through the heat exchanger.

Figure 9 Water chiller

4.1.8 Thermocouples

The temperatures at each inlet and outlet of the cores and shells of both heat exchangers were collected using type T thermocouples with a limit of error of 1.0 ℃ or 0.75% manufactured by Omega.

4.1.9 Viscometer

The Brookfield DV-I Prime Viscometer was used in order to measure the viscosity of MPCMs for this experiment as seen in Fig 10. The Brookfield viscometer has a guaranteed accuracy of +/- 1%. The relative error of a particular viscosity reading is relevant to the actual display (%torque) reading. The relative error improves as the reading approaches 100. The DV-I Prime is a rotary digital viscometer that displays the viscosity of the fluids on its LCD display. This viscometer is capable of continuous sensing and

display without requiring any attention by the user. This instrument can be connected to a PC or a printer for recording and storage of data.

Figure 10 Brookfield DV-I Prime viscometer

As the rotational speed increases, the drag increases. For a particular test fluid, the speed of the spindle is varied to determine the change in viscosity with respect to rotational

speed. Different kinds of spindles may be used to obtain different viscosity ranges. The viscometer used in this research work belongs to the LV series of viscometers from Brookfield.

4.1.10 Data acquisition system

The flow meters, pressure transducers and thermocouples were connected to an Agilent 34970A Data Acquisition&Switch Unit which collected data and made accessible through the Agilent BenchLink Data Logger 3 (Fig. 11) software.

Two Agilent data acquisition units were utilized to record data from thermocouples, pressure transducers, and flow meters. Agilent units of type 34970 A were used. Agilent Bench Link Data Logger software was used with the 34970 A for configuration and data analysis. The switching, conversion and reference junction errors of thermocouples were already taken into account by the unit.

Figure 11 Agilent 34970A data acquisition system

The arrangement of the heat transfer system is summarized in Fig. 13, where it can be seen the three different loops that are connected by the CHXs. From the analysis point of view, HX#2 was used for most calculations since it was where the PCM inside the MPCM slurries experiences crystallization. It is important to remark that the fluid running through the shell of HX#2 is called the cold fluid and the fluid running through the core is called the hot fluid. In order to complete the experiment, the cold fluid was always water for all the system tests, and the hot fluid was either water or MPCM slurries. All the components can be seen from Table 2.

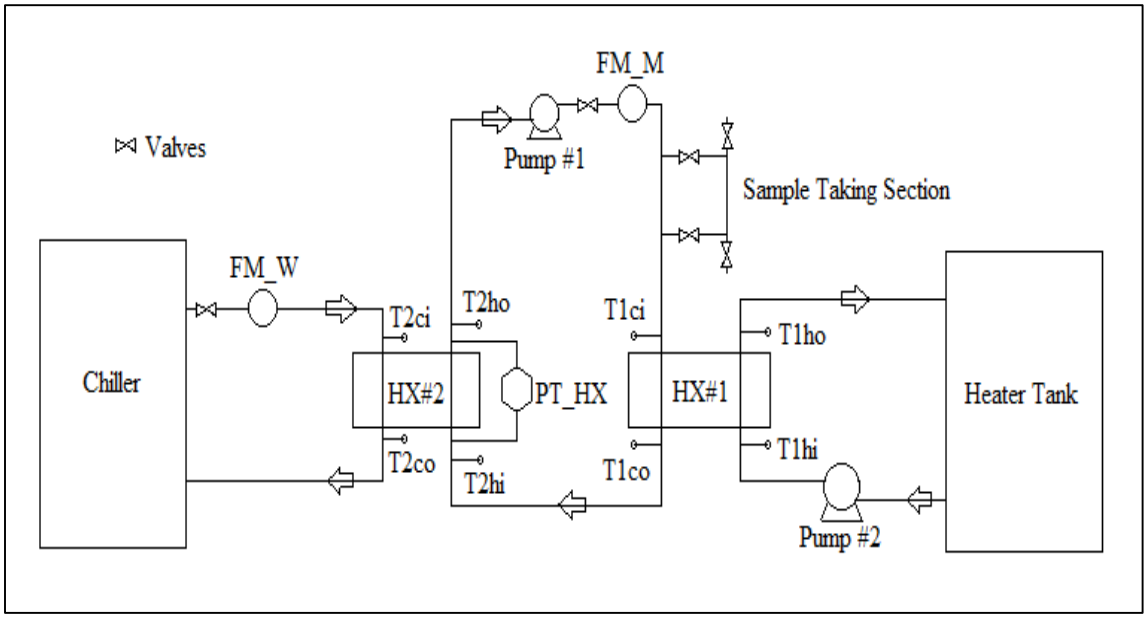

Figure 12 Experimental heat transfer diagram;

Table 2 Components and variables

Component	Variable	Component	Variable
Flowmeter in the loop that connect the CHXs	FM_W	thermocouple in the core's inlet of HX#1	$T_{1,c,i}$
flowmeter for the cold fluid in HX#2	FM_M	thermocouple in the core's outlet of HX#1	$T_{1,c,o}$
thermocouple in the shell's inlet of HX#2	$T_{2,c,i}$	thermocouple in the shell's inlet of HX#1	$T_{1,h,i}$
- thermocouple in the shell's outlet of HX#2	$T_{2,c,o}$	thermocouple in the shell's inlet of HX#1	$T_{1,h,o}$
thermocouple in the core's inlet of HX#2	$T_{2,h,i}$	pump of the loop that connect the CHXs	Pump #1
thermocouple in the core's outlet of HX#2	$T_{2,h,o}$	pump of the hot fluid in HX#1	Pump #2
pressure transducer	PT_HX		

4.2 Data reduction

To achieve the principal objectives of this research, there are other relevant variables that need to be found and analyzed, including density of PCM, latent heat of fusion of PCM, Reynolds number, and other temperature dependent properties. The properties were calculated to ensure that the system worked under the required conditions such turbulent regime and that the MPCM slurries could achieve complete phase change. The calculations of all the key parameters were performed using the Engineering Equation Solver (EES) software. The EES codes used for the calculations can be found in the Appendix.

4.2.1 Fluid properties

The fluid properties on the shell and coil sides were consistently evaluated at the mean temperature of their respective inlet and outlet temperatures using Equation (11).

$$T_m = \frac{T_i + T_o}{2} \tag{11}$$

The fluid properties of water were obtained from the NIST Theromphysical Property Database for water at 1 Atmosphere. Different methods were used to calculate the MPCM slurry properties due to the complex nature of the slurry. The viscosity of the slurry was measured in the laboratory using a rotary viscometer at three different shear rates to ensure Newtonian behavior.

The density of the MPCM slurry was measured and calculated using Equation (12). The sample of MPCM slurry was taken using the sample taking part. The weight of the wet MPCM slurry sample was taken and a heater was used to heat up the water in the sample until it completely evaporated. Then the mass of the dry MPCM slurry was measured which was used to estimate the mass fraction of MPCM using Equation (13).

$$\rho_{slurry} = \frac{Mass\ of\ \ MPCM_{wet}}{Volume\ of\ \ MPCM_{wet}} \tag{12}$$

$$MF = \frac{Mass\ of\ \ MPCM_{dry}}{Mass\ of\ \ MPCM_{wet}} \tag{13}$$

The latent heat of fusion of the MPCM was calculated and measured experimentally using a differential scanning calorimeter. Experimental differential scanning calorimetry (DSC) data of the MPCMs (Fig 13) shows that the latent heat of fusion of MPCM is between 136.4 and 152 kJ/kg.

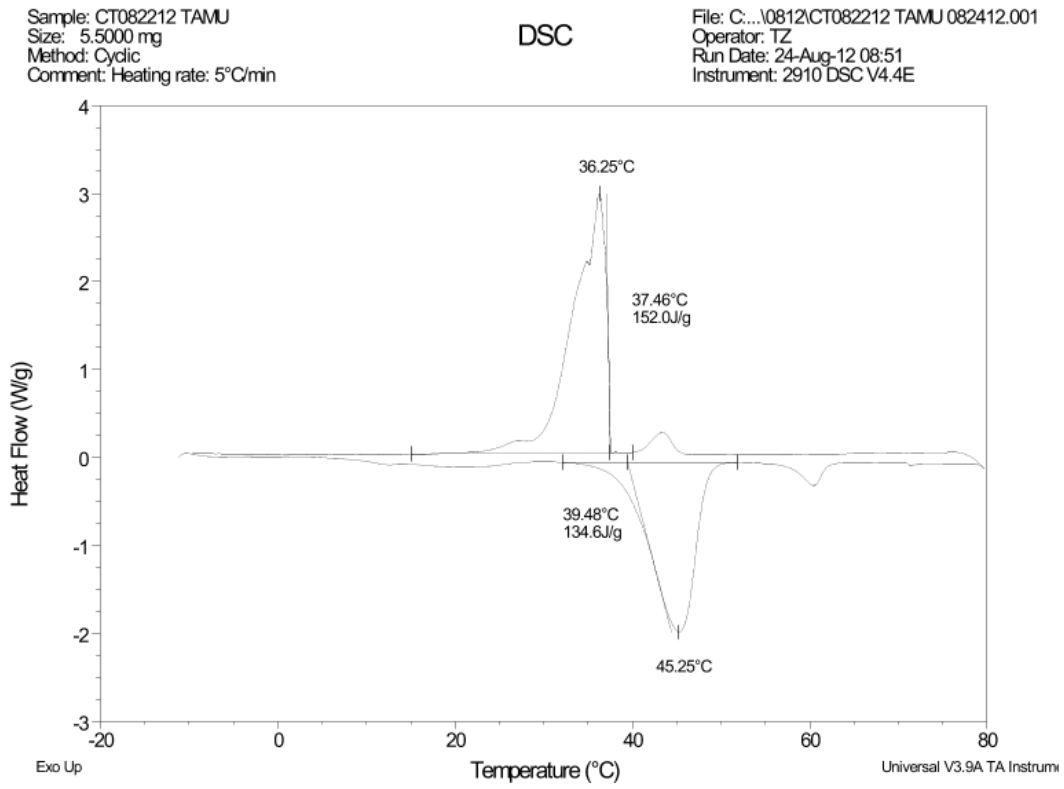

Figure 13 Differential scanning calorimetry data

To verify if MPCM particles in the slurries were undergoing complete or substantial phase change, Equation (14) was used by taking into account the DSC data including latent heat of fusion data. Equation 8 is based on energy balance as proposed by Alvarado et al. [3], where ϕ_{MPCM} is the fraction of MPCM particles undergoing phase change, MF_{MPCM} is the mass fraction of MPCM particles in the slurry and λ_{MPCM} is the latent heat of fusion of the MPCM particles.

$$\dot{Q} = \dot{m}_h \Delta T_h \left[(1 - MF_{MPCM}) c_{p,c} + MF_{MPCM} c_{p,h}\right] + \emptyset_{MPCM} (\dot{m}_h MF_{MPCM} \lambda_{MCPM}) \qquad (14)$$

4.2.2 Heat exchanger properties

The heat exchanger cross-section area consists of a core and an annulus. The outer part is a round duct and the inner part is irregular as it can be seen in Fig 14.

Figure 14 Inner shape of the coaxial heat exchanger

To be able to characterize heat transfer performance of MPCM slurry in coil heat exchangers, it is important to calculate the hydraulic diameter of the heat exchanger using Equation (15) as follows:

$$D_{hd,c} = \frac{d_{o,shell} + d_{i,shell}}{2} - D_{hd,\mathrm{h}} \tag{15}$$

The core side of the heat exchanger was used to pump MPCM through it. Since the outer surface of the core is very irregular, Equation (16) was used to estimate the hydraulic diameter of the core side.

$$D_{hd,h} = \frac{(d_{o,core} + d_{i,core})}{2} \tag{16}$$

The total heat transfer area can be calculated using Equation (17). The length of the core and inner annulus area can be obtained and calculated using Equations (18) and (19). Other parameters used in the calculations can be found in Table 2.

$$A_{sur} = \pi \cdot D_{hd,h} \cdot L_{hx,core} \tag{17}$$

$$L_{hx,core} = \frac{Vol_{hx,core}}{A_{i,h}} \tag{18}$$

$$A_{i,h} = \pi \times \left(\frac{d_{i,core}}{2} \right)^2 \tag{19}$$

The coil heat exchanger consists of a twisted tube that separates the core side from the shell side, as it can be seen in Fig 15. By inducing swirl flow on the tube side fluid, the twisted tube is used to enhance heat transfer which will offer a modest increase in heat transfer and cause low additional pressure loss. The low pressure drop characteristic is an ideal choice for turbulent flow.

Figure 15 Twisted tube (tape) enhancement

4.2.3 Log mean temperature equations

Because of the non-linear properties of the fluids when temperature changes in the heat exchanger caused by the phase change process, the average temperature difference, ΔT_m, should be determined to facilitate the heat transfer analysis. An energy balance was applied to the differential elements of the coil and the shell side fluids using Equations (20) and (21). In this present experiment, the coil side contains the hotter one of the two fluids, with C_h and C_c as the heat capacity rates of the respective fluids. The differential rate of heat transfer can also be calculated based upon a differential surface area, *dA*, using Equation (22) where ΔT is the local temperature difference calculated as $\Delta T = T_h - T_c$.

$$dq = -\dot{m}_h C_{p,h} dT_h = -C_h dT_h \tag{20}$$

$$dq = -\dot{m}_c C_{p,c} dT_c = C_c dT_c \tag{21}$$

$$dq = U\,\Delta T\,dA \tag{22}$$

In summary, the log mean temperature difference (LMTD) approach as seen in Equation (23) can be used to estimate the rate of heat transfer taking place within the CHX. Details of the LMTD approach can be found in Incropera [20].

$$q = UA\Delta T_{lm}$$

$$\Delta T_{\mathrm{lm}} = \frac{\Delta T_2 - \Delta T_1}{\ln(\frac{\Delta T_2}{\Delta T_1})} \tag{23}$$

4.2.4 Heat transfer equations

The Reynolds number was calculated to determine how it was affected by the concentration of the MPCM slurries and varying flow rates, and to verify if the flow satisfied the condition of turbulence. Alvarado et al. [3] explains that that Reynolds numbers below 2000 for most MPCM slurries are characterized as being laminar flow, while Reynolds numbers over 5000 are representative of turbulent flow. Reynolds number was calculated for the shell and core sections of the HX#2 using Equation (24) and Equation (25) respectively. In these equations ρ_c is the density of the cold fluid, V_c is the mean velocity of the cold fluid, $D_{hd,c}$ is the hydraulic diameter of the shell section of HX#2, μ_c is the viscosity of the cold fluid and μ_h, the viscosity of the hot fluid.

$$Re_{shell} = \frac{\rho_c \cdot V_c \cdot D_{hd,c}}{\mu_c} \tag{24}$$

$$Re_{core} = \frac{\rho_h \cdot V_h \cdot D_{hd,h}}{\mu_h} \tag{25}$$

The Dean number, which is a representation of the acting viscous forces in a fluid that goes through a curved pipe to the centrifugal forces [20], was calculated for the shell and core of the HX#2. The equations for these calculations are shown in Equation (26) and Equation (27), respectively. These numbers are used to determine how NTU and UA behave at different Dean Numbers based on experimental data.

$$De_{shell} = \mathrm{Re}_{shell} \times \sqrt{\frac{D_{hd,c}}{D_m}} \tag{26}$$

$$De_{core} = \mathrm{Re}_{core} \times \sqrt{\frac{D_{hd,\mathrm{h}}}{D_m}} \tag{27}$$

The pressure drop measurements are very important in order to fulfill the objectives of the study. The pressure drop between the inlet and outlet of the core in the HX#2 was used to determine how the MPCM concentration affects the friction factor f of the fluid inside the core. For this calculation, Equation (28) was used where $D_{H,h}$ is the hydraulic diameter of the core, ΔP_{HX} is the pressure drop measured, ρ_h is the hot fluid's density and V_h is the mean velocity of the hot fluid, which it is calculated from the volume flowrate divided by the area inside the pipe as seen in Equation (29).

$$f = \frac{2 \cdot D_{H,c} \cdot \Delta P_{HX}}{\rho_h \cdot L_{HX} \cdot {V_h}^2} \tag{28}$$

$$V_h = \frac{V_{fl,h}}{A_{i,h}} \tag{29}$$

4.2.5 Heat exchanger effectiveness

The overall heat transfer coefficient U was used to determine the thermal behavior of the CHX when the concentration of the MPCM slurries and the flow rate were varied. UA was calculated using Equation (30) where q_{act} is the actual heat transfer rate and ΔT_{lm} is the log mean temperature difference for counterflow configuration. Q_{act} was calculated based on energy balance by knowing the amount of heat being transferred to the single phase fluid, in this case, water.

$$U = \frac{q_{act}}{\Delta T_{lm} \cdot A_{sur}} \tag{30}$$

The UA value was used to calculate the number of heat transfer units (NTU) as in Equation (31) where C_{min} is the minimum heat capacity between the hot fluid's heat capacity and the cold fluid's heat capacity.

$$NTU = \frac{UA}{C_{min}} \tag{31}$$

The heat capacity is the product of the mass flow rate of the fluid and the fluid's specific heat which for water was calculated using an EES function based on the fluid's temperature and pressure. On the other hand, the specific heat of the MPCM slurries varies with through the CHX, being this reason why there is insufficient data to calculate the heat transfer rate from the hot fluid's data alone.

The heat transfer rates q_c calculated from the cold fluid's data, and q_h calculated from the hot fluid's collected data are very important in this study in order to obtain the effectiveness of the CHX (ε_{HX}). For the system tests when water was running through the core and shell of the CHXs these values were obtained from Equation (32) and Equation (33), respectively, where $\dot{m}_c$ is the mass flow rate of the cold fluid, $\dot{m}_h$ is the mass flow of the hot fluid, $c_{p,c}$is the specific heat of the cold fluid, $c_{p,h}$ is the specific heat of the hot fluid, ΔT_c is the absolute temperature difference of the cold fluid between inlet and outlet of the shell section, and ΔT_h is the absolute temperature difference between the inlet and outlet of the core section. With these, it can be determined if the system is working and if the calculations are accurate by calculating the percentage of difference between these two values. Otherwise, for the MPCM slurries, as explained before, the specific heat cannot be specified. Then for this analysis it is assumed that q_c and q_h are the same value and the specific heat of the MPCM slurry is obtained solving for $c_{p,h}$ in Equation (33).

$$q_c = \dot{m}_c \cdot c_{p,c} \cdot \Delta T_c \tag{32}$$

$$q_h = \dot{m}_h \cdot c_{p,h} \cdot \Delta T_h \tag{33}$$

The effectiveness of the CHX is equal to the quotient of the actual heat transfer rate q_{act} and the maximum possible heat transfer rate q_{max} as it is shown in Equation (34). For the water tests, q_{act} is the minimum heat transfer rate calculated. For the MPCM slurries tests, q_{act} was based in the water side data. q_{max} was calculated using Equation (35) where $T_{2,h,i}$ is the temperature at the core's inlet of the HX#2 and $T_{2,c,i}$ is the temperature at the shell's inlet of the HX#2.

$$\varepsilon_{HX} = \frac{q_{act}}{q_{max}} \tag{34}$$

$$q_{max} = C_{min} \cdot \left(T_{2,h,i} - T_{2,c,i}\right) \tag{35}$$

4.3 Calibration and validation

In order to obtain accurate and reliable values from the system, the thermocouples were calibrated before running the experiments. The calibration was conducted with water running through the whole system and under steady state with no heat flux added or subtracted. Under these conditions the thermocouples should register the same temperature. To ensure that, an average of each thermocouple was taken, then a grand average was calculated from them and finally the calibration factors of each thermocouple were obtained subtracting the average value of each one of them from the grand average value. The resulting values, positives or negatives, were introduced in the Agilent BenchLink Data Logger 3 software as offset values.

Then, experimental tests with water in the whole heat transfer system were conducted to validate the properly operation of the system before pouring MPCM slurries in it. In order to complete the validation the heat transfer rate was calculated using the collected data from the shell side and core side. Then a percentage of difference between them was obtained to verify if they were close enough because they, by theory, should be the same. With this method, a maximum difference of 6.0% was obtained between both heat transfer rates which suggests a good behavior of the heat transfer system when MPCM slurries experiments were conducted.

5. RESULTS AND DISCUSSION

A number of heat transfer experiments were conducted using MPCM slurries as heat transfer fluids using a coil heat exchanger (CHX). The results from the heat transfer tests are presented below.

5.1 MPCM slurries properties

The MPCM slurry used in the experiments was manufactured by Thies Technology Inc. The product ID given to the slurry was CT082212 TAMU. The initial mass fraction of the slurry was 17.8% with water as carrier fluid.

Table 3 MPCM properties (LHF stands for latent heat of fusion)

Fluids	Properties						
	Viscosity [cP]	Density [kg/m^3]	c_p [J/(g·°C)]	Melting point [℃]	Crystallization Point [℃]	LHF under Melting [J/g]	LHF under Crystallization [J/g]
4.6% MPCM	1.67	947	5.23	39.48	37.46	134.6	152.0
8.7% MCPM	1.86	845.8	6.13				

A differential scanning calorimetry (DSC) experiment was conducted and the results revealed that the melting point of the MPCM is 39.48 ℃ and crystallization point

is 37.46°C. Also, from the DSC data it can be taken the MPCM's latent heat of fusion under melting is 134.6 J/g while the latent heat of fusion under crystallization is 152.0 J/g. In order to conduct the heat transfer experiments at lower mass fraction of MPCM, the mass fraction of MPCM slurry was decreased by simply adding more water. For this, an estimate of the system's volume was made and then it was filled the correspondent amounts of MPCM and water to achieve the desired mass fraction. The process was made twice before conducting each experiment, to achieve mass fractions of 4.6% and 8.7%, respectively. Both mass fraction levels were used to Newtonian behavior [7].

To complete the analysis of the properties of MPCM slurry, the density and viscosity of the new slurries was measured and calculated. The density of the 4.6% mass fraction slurry was measured to be 947.0 kg/m^3 and for the 8.7 % mass fraction slurry, 845.8 kg/m^3. The viscosity of both slurries was measured using a Brookfield viscometer at temperatures and at a spindle rate of 100 rpm. The temperature points were chosen taking in consideration the maximum and minimum temperatures reached by the MPCM slurries during the experiments. The results of these measurements are shown in Fig 16. The trend of the viscosity fits well when compared with previous studies [7]. For the further analysis of the experiments conducted using the heat transfer system, averages of the viscosity values were used to estimate Reynolds and Dean number values within the CHX.

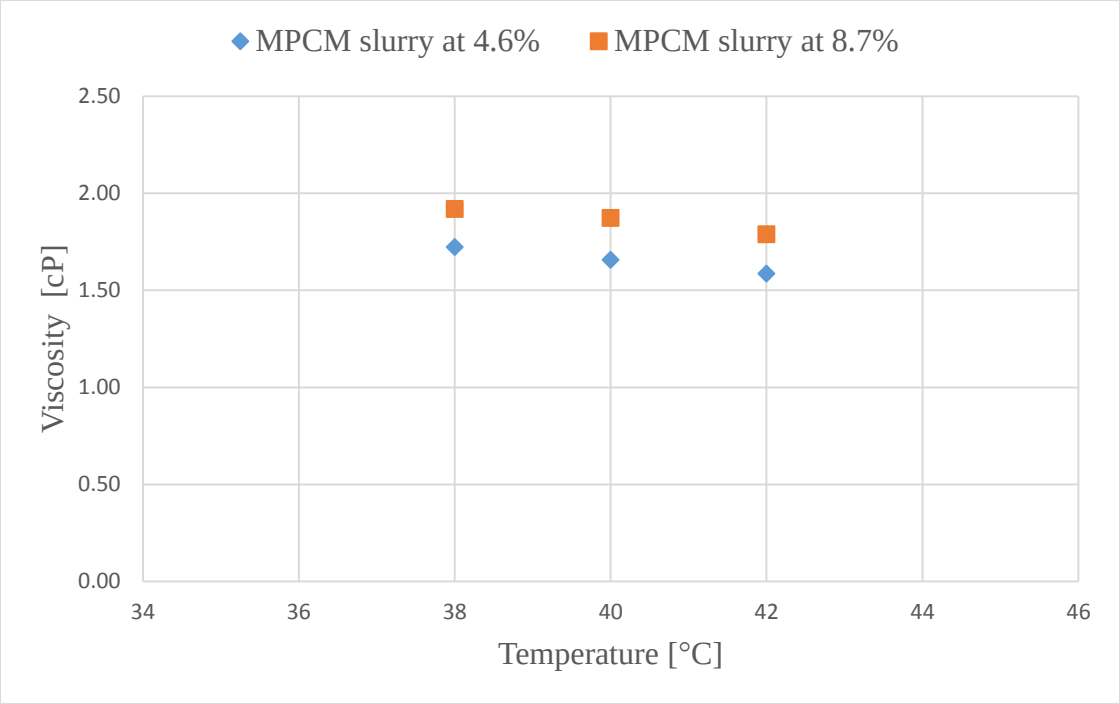

Figure 16 MPCM viscosity (cP) for different mass fraction

5.2 Heat transfer test conditions when using water and MPCM slurries as heat transfer fluids

5.2.1 Water in shell and water in core test

For the case when water was used as heat transfer fluid on the core and shell sides, there were a total of 7 runs with different flowrates varied from 7 l/min to 10 l/min. The raw data for these runs can be seen in Table 3. The total calculated heat load varied from 2.6 – 4.0 kW. Proper energy balance calculations were undertaken and only an average of 4.0 % discrepancy between the shell side and coil side were found.

Table 4 Flowrates and temperature data for the case of water in shell and core sides

Test Numbers	Hot Water Side		Cold Water Side		Hot Water	Cold Water
	T_{2hi} (℃)	T_{2ho} (℃)	T_{2ci} (℃)	T_{2co} (℃)	$V_{fl,,h}$ (L/min)	$V_{fl,,c}$ (L/min)
1	40.9	35.2	32.1	37.4	7.1	7
2	41	35.3	32.1	37.6	7.4	7.5
3	41	35.3	32.2	37.6	8	8.1
4	41.1	35.3	32.2	37.7	8.5	8.5
5	41.1	35.4	32.3	37.8	9	9
6	41.2	35.4	32.3	37.9	9.5	9.5
7	41.2	35.4	32.2	37.9	10	10

5.2.2 Water in shell and MPCM (4.6% and 8.7% mass fraction) in core test

The second part of the experimental plan involves using water in the shell and MPCM slurries (two different mass fraction) in the coils to assess the effectiveness of the CHE when MPCMs were used. Seven runs for each tests were conducted. The volumetric flowrates were similar to that in the first part of the experimental plan. The as-recorded data can be seen in Table 5 and Table 6. Equation (8) was used to determine the phase change percentage of MPCM slurry.

Table 5 Flowrates and temperature data for the case of water in shell with MPCM (4.6%) in the coils

Test Numbers	MPCM Side		Water Side		MPCM	Water	ϕ_{MCPM}
	T_{2hi} (℃)	T_{2ho} (℃)	T_{2ci} (℃)	T_{2co} (℃)	$V_{fl,h}$ (L/min)	$V_{fl,c}$ (L/min)	
1	40.7	35.6	32.1	38.2	7	7	85%
2	40.8	35.6	32.2	38.3	7.4	7.6	90%
3	40.9	35.7	32.2	38.4	8	8	86%
4	40.9	35.7	32.3	38.5	8.5	8.5	86%
5	41	35.8	32.3	38.6	9.1	9	88%
6	41.2	35.7	32.2	38.7	9.5	9.5	87%
7	41.2	35.7	32.3	38.8	10	10	87%

Table 6 Flowrates and temperature data for the case of water in shell with MPCM (8.7%) in the coils

Test Numbers	MPCM Side		Water Side		MPCM	Water	ϕ_{MCPM}
	T_{2hi} (℃)	T_{2ho} (℃)	T_{2ci} (℃)	T_{2co} (℃)	$V_{fl,h}$ (L/min)	$V_{fl,c}$ (L/min)	
1	41.3	35.9	32.1	38.9	7.1	7	85%
2	41.2	35.8	32.2	38.9	7.4	7.5	88%
3	41.5	35.8	32.2	39.1	8	8.1	87%
4	41.4	35.9	32.2	39.1	8.5	8.5	89%
5	41.4	36	32.3	39.2	9	8.9	90%
6	41.6	35.9	32.2	39.3	9.5	9.6	94%
7	41.5	35.9	32.2	39.3	10.2	10.2	94%

It can be seen that the inlet and outlet temperatures were very similar to the water-to-water case. This temperature range was chosen for the cold side and hot side to ensure complete crystallization or melting of the phase change material inside each microcapsule. The outlet and inlet temperature of the MPCM slurry was set on average 2-3 ℃ lower and higher than the DSC data results, respectively, to make sure complete phase change of the MPCM particles was always achieved. The accurate phase change percentage of MPCM was calculated using Equation (7) and the results can be seen in Fig 17. As we can see from the figure, the phase change percentage were among 90%, so it was fair to assume the MPCM were underwent complete phase change. The highest phase change percentage was achieved when the flowrate reached the maximum, this is because when flowrate increase, the amount of heat rate transfer also increased facilitating the phase change process when using the CHX.

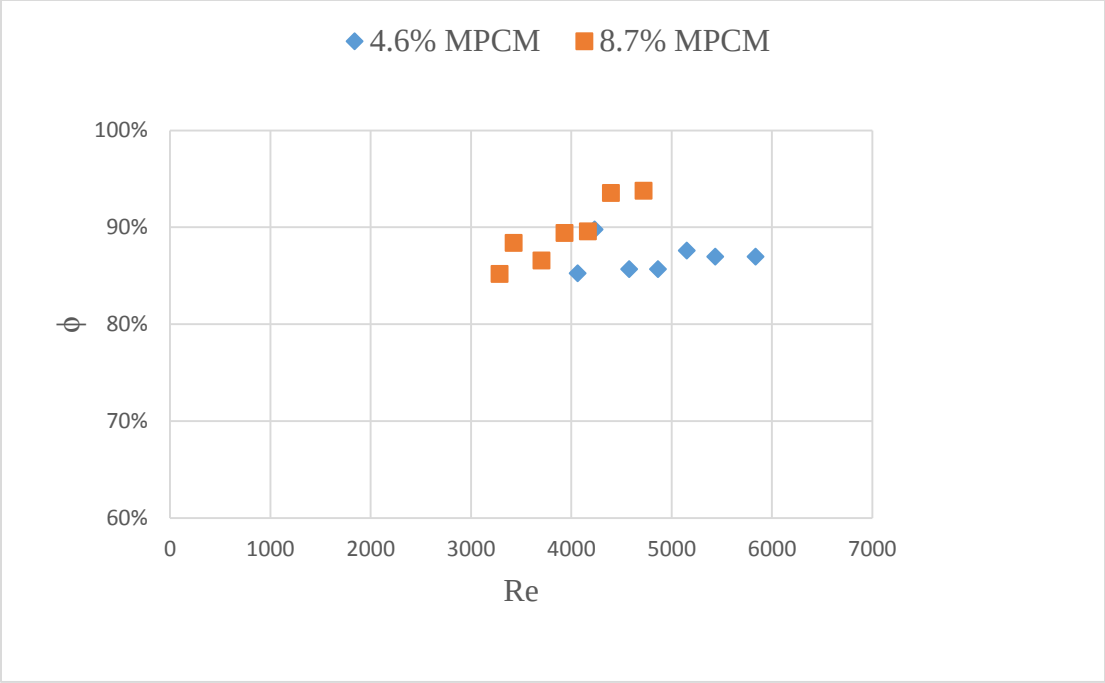

Figure 17 Percentage of phase change in MPCM

5.3 Reynolds number and dean number of heat transfer fluids in CHX

The Reynolds numbers in the core and shell were expected to be turbulent flow for all the tests. In Fig 18, it can be seen that the Reynolds number in the core (where MPCM flow through) reached turbulence for all the three tests, but it is obviously that the Reynolds number for water-water test is much higher than that of water-MPCM test, either 4.6% mass fraction or 8.7% mass fraction cases. This behavior of Reynolds number is due to the high kinematic viscosity of the MPCM slurry when compared with water. Even though the Reynolds number reached values as low as 3200, the flow most likely depicted turbulent-like behavior because of the nature of the twisted tube inside the CHX. The Dean number also depicts the same trend as of the Reynolds number which can be seen in Fig

19. Further analyses of the heat transfer process using Reynolds number and Dean number are presented below.

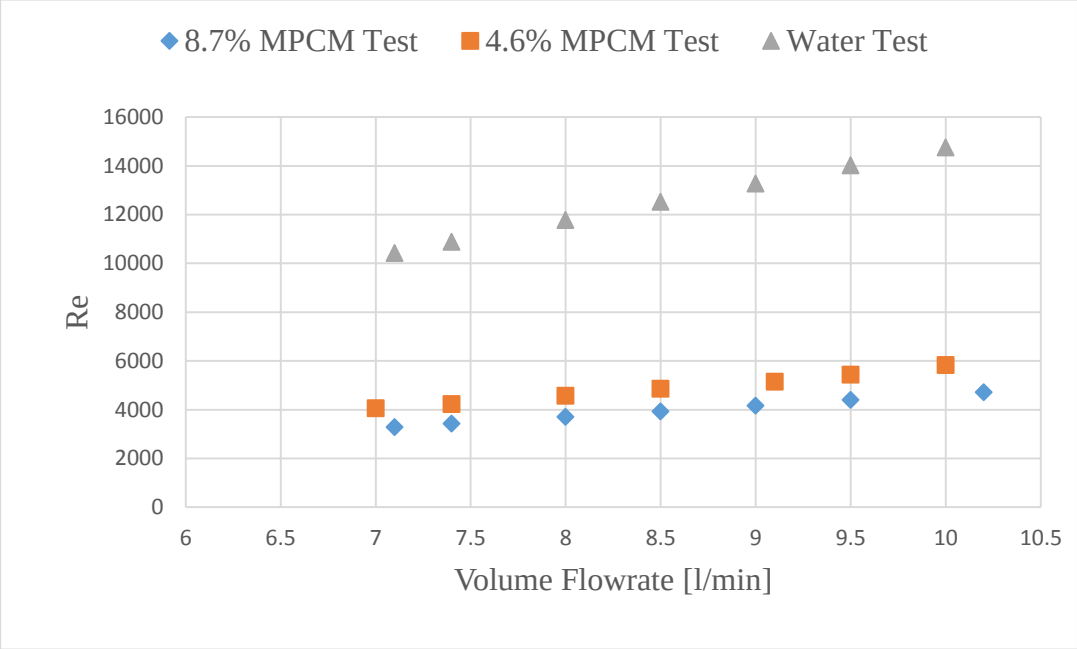

Figure 18 Reynolds number of heat transfer fluid in CHX

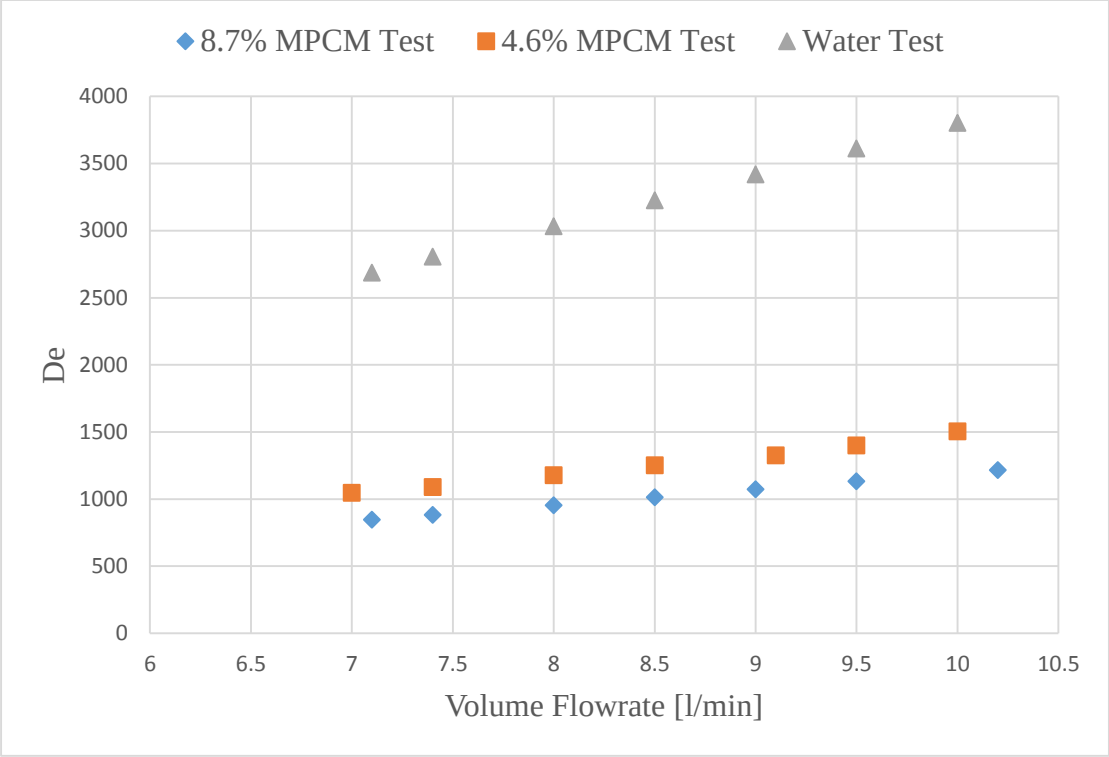

Figure 19 Dean number of heat transfer fluid in CHX

5.4 Pressure drop of heat transfer fluids in CHX

Flow experiments have been conducted to determine the pressure drop of MPCM slurry for two mass fractions. The data were collected along with temperature when the slurry reached steady-state conditions. Fig 20 shows the pressure drop results for MPCM at different mass fraction as well as for water at the same flow conditions. It can be seen that pressure drop increases slightly for MPCM test even though the viscosity is about two to three times higher than for water. Therefore, MPCM should not significantly affect pumping power. These phenomena might suggest the presence of drag reduction effect between the MPCM slurry and the inner surfaces of the CHX.

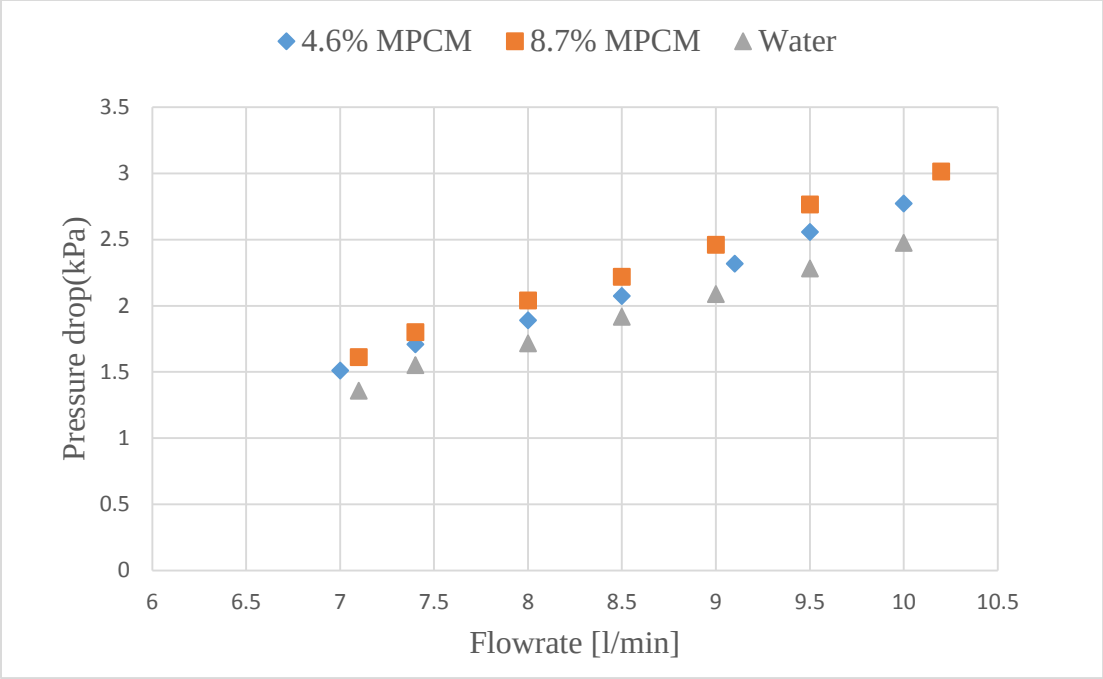

Figure 20 Pressure drop of heat transfer fluids in coil heat exchanger

By using pressure drop data, the corresponding friction factor values for different Reynolds number were determined and plotted as shown in Fig 21. Given the complex internal configuration of the CHX, a Blasius-type friction factor equation was used to estimate friction factor as a function of Reynolds by using the following equation:

$$f = a \cdot \mathrm{Re}^{-b} \tag{36}$$

From Fig.21, it can be seen that the friction factor values decrease with Reynolds as expected for any Newtonian fluid under turbulent-like conditions. The high friction factor values are attributed to the effect of the twisted tube on pressure drop. The experimental friction factor values were correlated using Equation as shown in Fig. 21 and Table 7. Given the relatively high correlation factor (R^2), it can be concluded that

the friction factor can be estimated using Equation (36) for MPCM slurries at fixed mass fraction values.

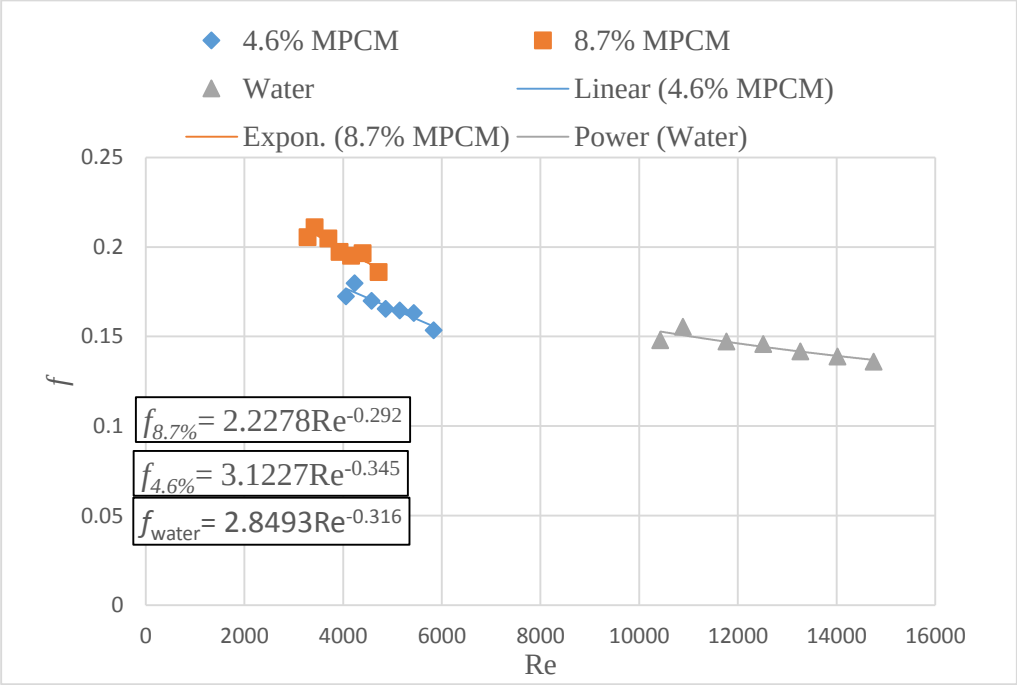

Figure 21 Friction factor as a function of Reynolds number

Table 7 Friction factor correlation variables

Fluid	***a***	***b***	R^2
Water	2.85	0.32	0.82
MPCM （4.6%）	3.12	0.35	0.84
MPCM （8.7%）	2.23	0.29	0.85

From Fig. 21, it is evident that mass fraction has an effect on friction factor. Furthermore, each correlation shown in Fig.21 and Table 7 can only be used for a specific mass fraction. A general friction factor correlation has been developed as seen in Equation (37) that can be used for any MPCM slurry in a CHX.

$$f = \mathrm{a} \cdot \mathrm{Re}^{-b}(1 - MF)^{-c} \tag{37}$$

where *MF* stands for mass fraction of MPCM slurry as defined by Equation 8 in Section 4.

By using the regression method, the parameters in Equation (37) have been determined as seen in Table 8.

Table 8 Variables for the general fraction factor correlation

a	***b***	***c***	$\boldsymbol{R^2}$
0.276	0.07	2.62	0.91

Equation 31 can be used to calculate the friction factor as a function of Reynolds number for one specific fluid but it cannot be extended to other fluids unless it is fitted using experimental data. However, Equation 32 can be used for any MPCM slurry in a CHX. From Table 8, it is clear that MPCM mass fraction plays a more significant role in dictating the magnitude of the friction factor rather than Reynolds number.

5.5 CHX heat transfer results for water and MPCM slurries

One of the objectives of the project was to quantify the heat exchanger effectiveness of the devised CHX. For that purpose, inlet and outlet temperatures as well as heat transfer rates were measured and calculated to determine effectiveness using the ε-NTU method. However, to be able to use the ε -NTU method, the overall heat transfer coefficient for the whole CHX had to be determined first when water was flowing through the coil and shell sides. Therefore, the shell side overall heat transfer coefficient was calculated as explained above using the data shown in Table 2. The results can be seen in Fig 22. It can be noticed that the U increased 23% on average between water test and MPCM at 4.6% mass fraction test, but the difference is only about 8% between MPCM at 8.7% mass fraction and at 4.6% mass fraction. The temperature differences were kept the same during these experiments. The reasons why the overall heat transfer coefficient of MPCM slurry is higher than for water can be attributed to the latent heat of fusion of the phase change material within the MPCM. From the figure below, it is evident that the maximum overall heat transfer enhancement occurs when the flowrate reaches its maximum value. Furthermore, overall heat transfer coefficient increases with MPCM mass fraction.

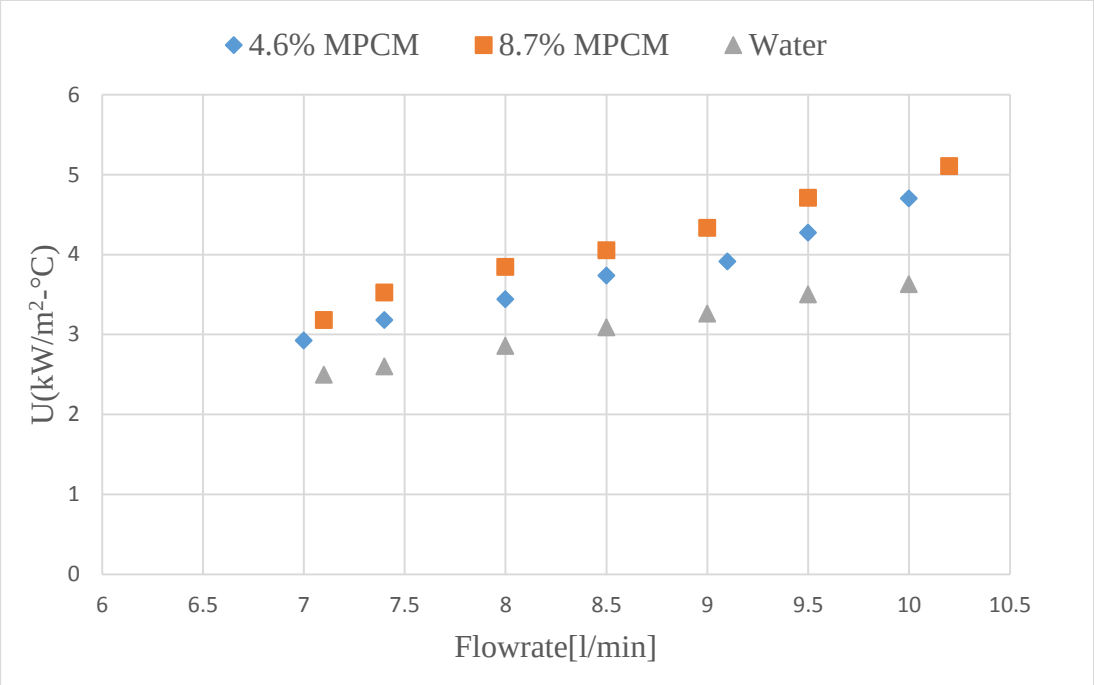

Figure 22 Overall heat transfer coefficient as function of flowrate

Fig 23 shows how the overall heat transfer coefficient varies with Reynolds number. The figure also shows lower Reynolds number for MPCM slurries because MPCM viscosity is proportional to mass fraction.

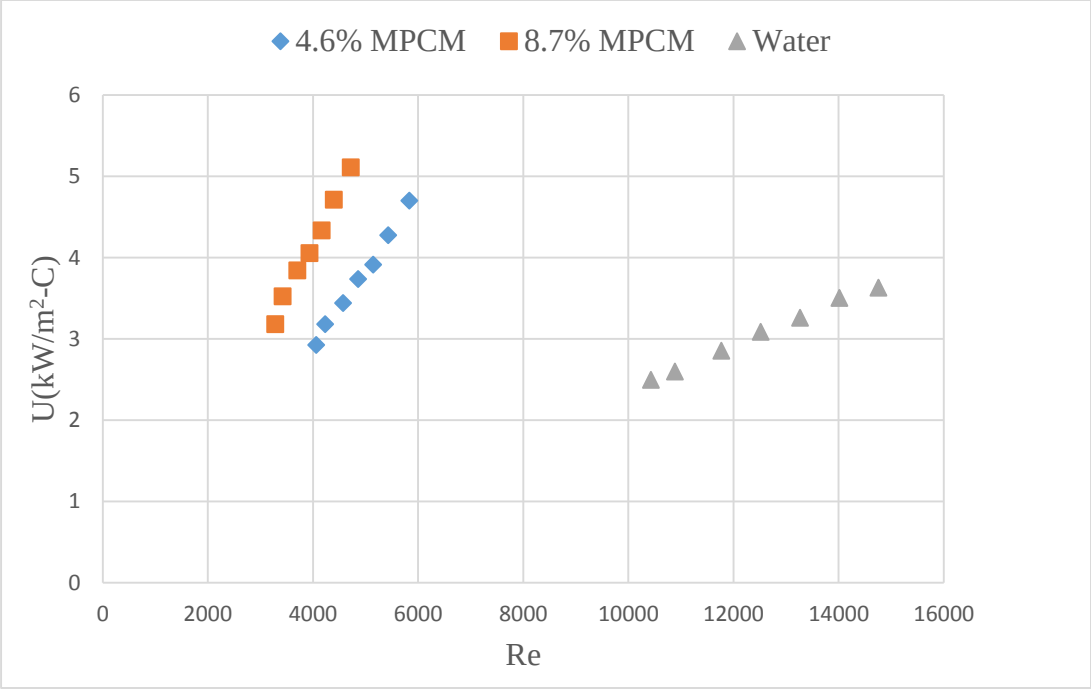

Figure 23 Overall heat transfer coefficient as a function of Reynolds number

It is important to find out whether the high or low concentration of MPCM leads to greater thermal efficiency. The performance efficiency coefficient (PEC) as seen in Equation (38) is used to determine MPCM slurry lead to PEC greater than 1 when compared to water as heat transfer fluid.

$$PEC = \frac{\left(\frac{UA_{MPCM}}{UA_{water}}\right)}{\left(\frac{f_{MPCM}}{f_{water}}\right)} \tag{38}$$

In order to determine the effect of MPCM mass fraction on overall performance (PEC), it is necessary to determine its effect on UA_{ratio} and f_{ratio} individually. The UA_{ratio}

is the ratio of UA values for MPCM and water. The f_{ratio} is the ratio of friction factor values for MPCM and water. The effects of MPCM mass fraction and flow rate on UA_{ratio} and f_{ratio} can be seen in Fig 24 and Fig 25, respectively.

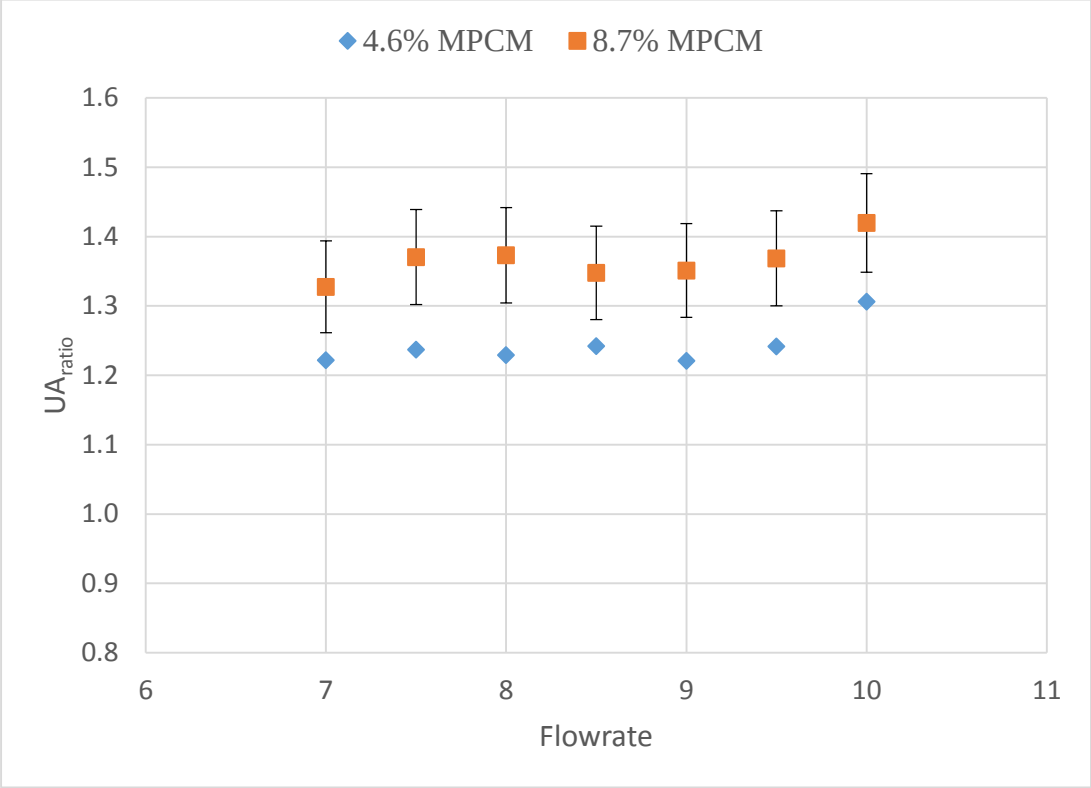

Figure 24 UA_{ratio} at different MPCM slurry flowrate

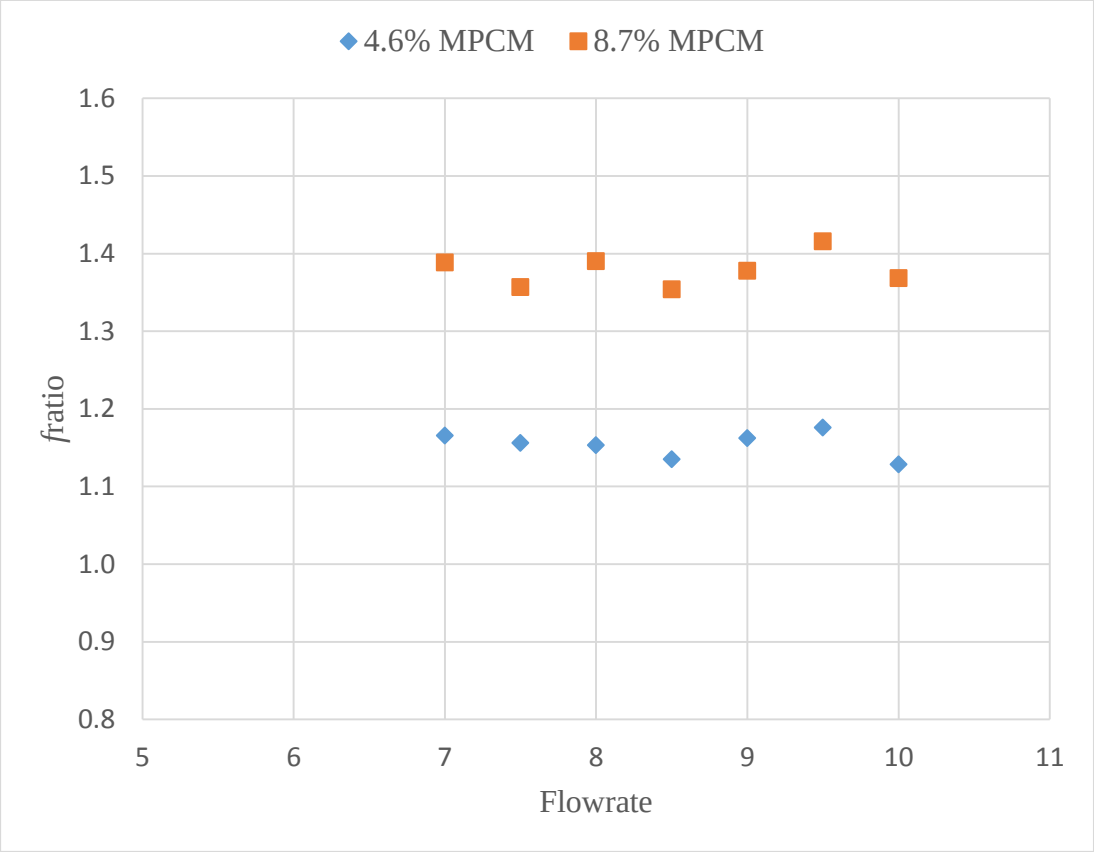

Figure 25 Friction factor ratio at different MPCM slurry flowrate

The UA_{ratio} and f_{ratio} for 8.7% mass fraction of MPCM are higher than for 4.6% mass fraction of MPCM. When both ratios are combined, PEC ratio can be obtained as shown in Fig 26. The PEC results for 8.7% MPCM is about 9% lower than that of 4.6% MPCM. It can be concluded that the lower mass fraction does have higher overall efficiency performance because the MPCM slurry at higher mass fraction is characterized by exhibiting higher pressure drop. By using PEC values, MPCM slurries at different mass fractions can be evaluated from the energy efficiency point of view.

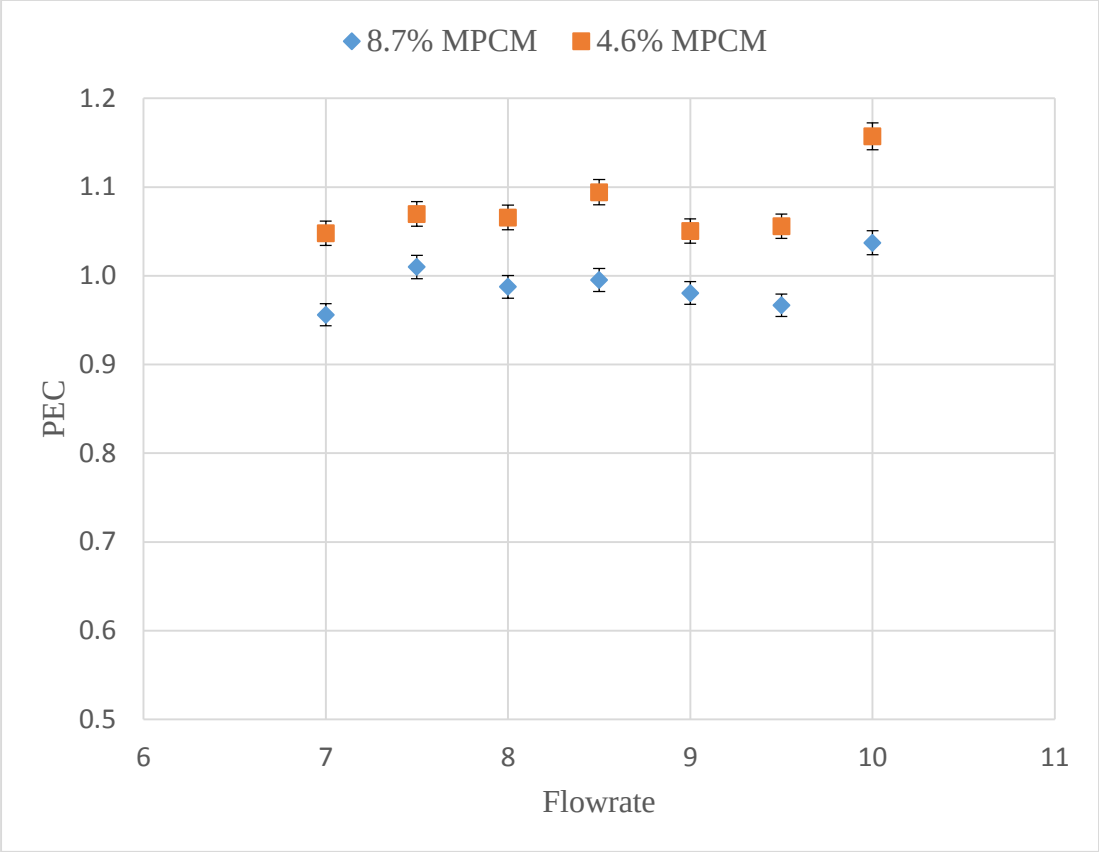

Figure 26 PEC values of MPCM slurry at different flowrates

The finding that heat transfer of MPCM slurry is greater than for water in a CHX can be further analyzed when the NTU value are compared as seen in Fig 27. From the figure, it is evident that NTU values are higher for MPCM slurry than for water because of the greater UA values that make up NTU. Furthermore, lower Reynolds number values are lower because of higher viscosity values of the MPCM slurries. In summary, the additional heat capacity contained within the MPCM slurry leads to greater amount of heat transfer within the CHX.

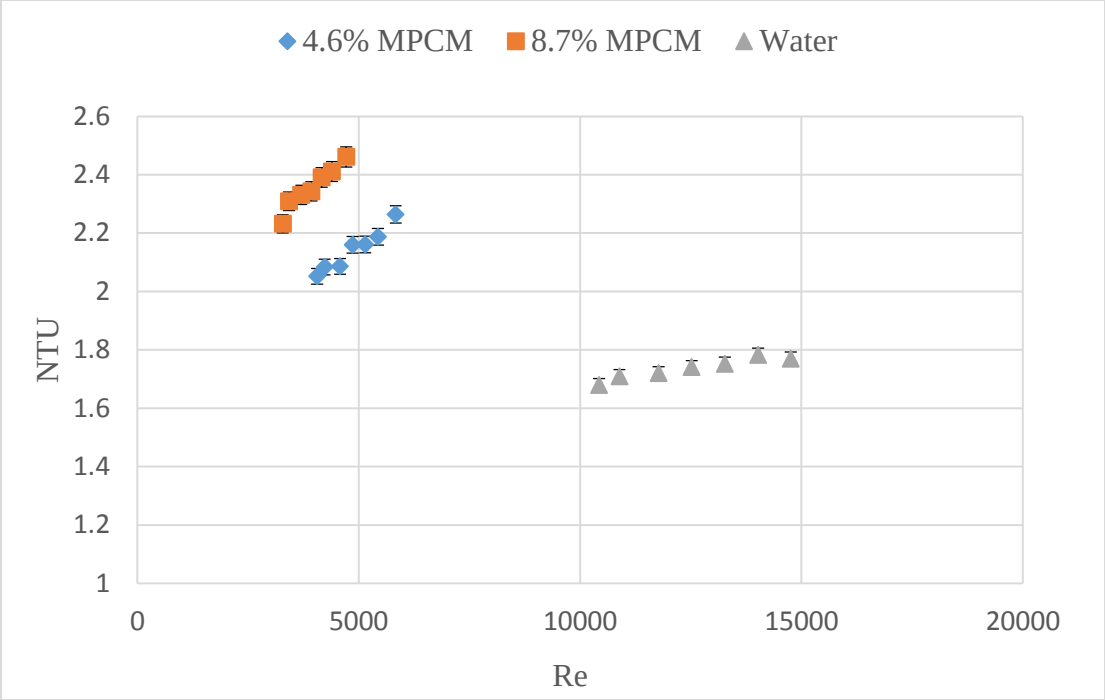

Figure 27 NTU of MPCM slurry at different Reynolds number values

The calculated effectiveness values as a function of NTU for all tests conducted during this study are depicted in Figure 28. The MPCM slurry data correlate well with the explicit ε-NTU relationship as shown in the figure. It is interesting to note that water depicts slightly lower effectiveness than the theoretical curve when Cr is set to 1 for counter flow, which is calculated From Equation (39).

$$\varepsilon = \frac{NTU}{1+NTU} \quad (C_r = 1) \tag{39}$$

The minimum heat exchanger effectiveness for a counter-flow configuration is found when Cr is set to 1. In the case of water tests, the Cr values were slightly lower than one as predicted by Equation (40) because of the small difference between C_c and C_h on the cold side and hot side of the heat exchanger, respectively. The optimal effectiveness values can be found when Cr is set to 0, or when phase change such as condensation or evaporation takes place within the CHX. From the MPCM tests, it is evident that MPCM slurry Cr values fall between 0 to 1. In order to determine the corresponding Cr values for the MPCM slurries, Equation 35 has been used to calculate their theoretical values and effectiveness curves.

$$\varepsilon = \frac{1-exp[-NTU(1-C_r)]}{1-C_r exp[-NTU(1-C_r)]} \quad (C_r < 1) \tag{40}$$

From Fig 28, it can be seen that the Cr of MPCM slurry are about 0.83 and 0.8 for 4.6% and 8.7% mass fraction, respectively. Evidently, the Cr value is less than one because the MPCM slurry side would always have greater heat capacity than the water side due to the latent heat of fusion of the phase change material in MPCM. This in turn has an effect of CHX effectiveness, which is greater than for water. This suggests that MPCM slurry under the right conditions (i.e. flowrate and mass fraction) can perform well from the heat transfer point of view.

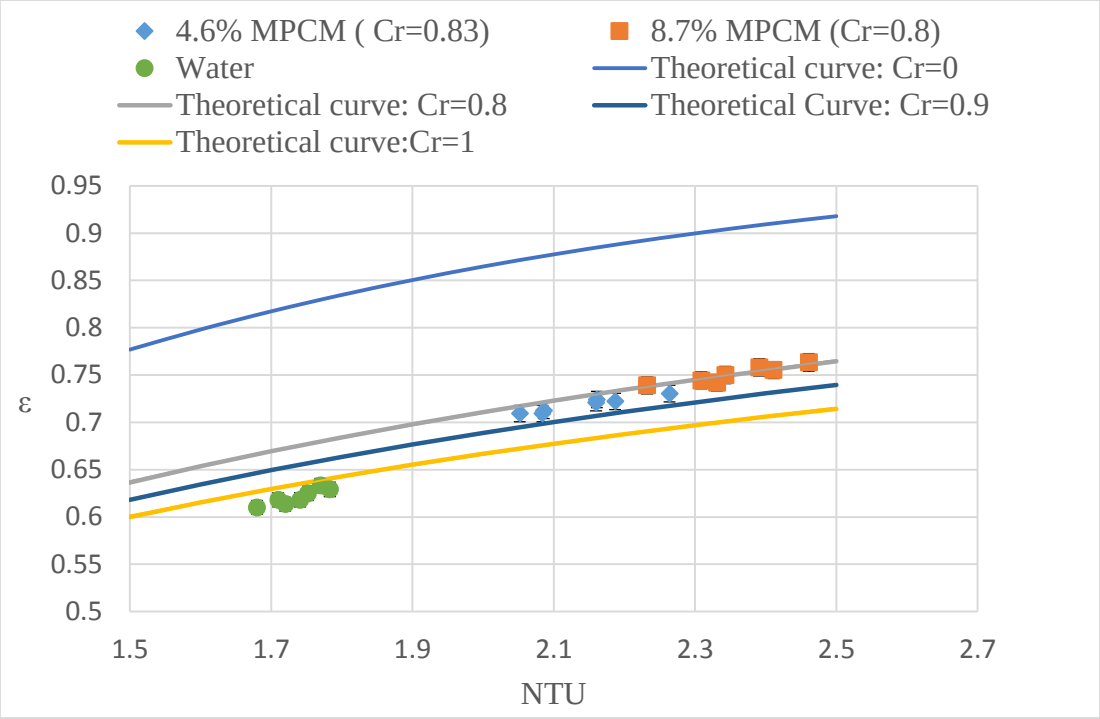

Figure 28 Heat exchanger effectiveness for different fluids and conditions

It remains to be seen in MPCM particles in the CHX contribute positively or negatively to the overall convection process if phase change within the MPCM does not happen. In single-phase helical coil flow, centrifugal forces impart a lateral movement of the inner core fluid to the outside edge of the coil possibly resulting in a circulatory process within the CHX. Because of this possible circulating movement that can be present even in the laminar regime, it is plausible that much more of the MPCM particles are able to interact with the wall and transfer their heat to the shell side fluid which wouldn't otherwise occur in straight tube laminar flow.

Analysis of the results should also take into account that the heat exchanger used in the present experiment was built quite differently from other helical coil. Because of this difference, we can assume there are other possible convective heat transfer mechanisms that should be explored by conducting a thorough study with single phase fluids first. Other factors that should be considered in the future include the collection of the temperature profile along the coil especially with the part when MPCM are undergoing phase change process.

Another assumption made during the analysis was the use of an effective specific heat for MPCMs that takes into account the latent heat of fusion. The Equation (8) is normally used to calculate specific heats while the MPCMs are undergoing phase change. In the present case, the MPCM slurry will spend a fixed amount of time as a multiphase fluid over an unknown length of coil, while the rest of the time it is assumed to be in the single-phase regime. Because the temperature range from the inlet and outlet of the coils covers both regimes and there is no data available to indicate when and where the phase change process occurs. Therefore, the total coil temperature difference must be used in the calculation of the effective specific heat which makes it difficult to assess the effect of phase change during the whole heat transfer process. Nevertheless, the data suggests that the devised CHE does improve the rate of heat transfer of MPCM slurries when compared to straight heat transfer sections.

6. CONCLUSION

The present experimental study has shown using MPCM slurry results in increases in heat transfer in a CHX. An initial set of tests were conducted in a coaxial coil heat exchanger (CHX) using water in the shell and water in coils in order to get a standard for this test system and for further comparison. Then second set of tests involving two different mass fraction of MPCM slurry in the coils were conducted in order to understand the effects of using MPCM slurry on heat transfer in a CHX. Increases in heat transfer seem to be largely affected by the thermal properties of MPCM. For this study work, the maximum heat transfer occurs when the core side flowrate reached the highest at the higher MPCM mass fraction.

The experimental results indicate that an optimal mass fraction of MPCM slurry leads to enhanced heat transfer performance even though there is a penalty in terms of pressure drop. The results also indicate that MPCM can perform better than water if the right conditions are imposed. In summary, a coil heat exchanger is certainly a good heat exchanger configuration to harness the potential of MPCM slurry as a heat transfer fluid.

In order to more reliably study the effects of the use of MPCM slurry in helical heat exchangers, a numerical simulation of the present study is recommended. The numerical study itself would not require any of the correlations used in the present analysis and could possibly provide a more accurate understanding of the present heat exchanger. Though taking into account micro particles in the fluid can be numerically cumbersome and time consuming, the effects of phase change can be taken into account

using well known heat capacity models. After this numerical analysis is complete, the results can be easily compared to the present study. Future studies should focus on providing the constant heat flux and maintain the temperature profile along the coil. With these variable, correlations in terms of MPCM's concentration, Dean number, heat capacity, coil's configuration would be developed to predict the heat transfer characteristics of MPCM slurries in a coil heat exchanger. It would be in great help in understanding the whole heat transfer process. The present study as well as any future studies on helical coil heat exchangers involving MPCM slurries will help strengthen the field of fluid dynamics and heat transfer in the quest for superior heat transfer methods.

REFERENCES

[1] Yamagishi, Y., Takeuchi, H., Pyatenko, A. T., 1999, "Characteristics of Microencapsulated PCM Slurry as a Heat-Transfer Fluid," AICHE Journal, **45**(4) pp. 696-707.

[2] Hu, X., and Zhang, Y., 2002, "Novel Insight and Numerical Analysis of Convective Heat Transfer Enhancement with Microencapsulated Phase Change Material Slurries: Laminar Flow in a Circular Tube with Constant Heat Flux," International Journal of Heat and Mass Transfer, **45**(15) pp. 3163-72.

[3] Alvarado, J. L., Marsh, C., Sohn, C., 2007, "Thermal Performance of Microencapsulated Phase Change Material Slurry in Turbulent Flow Under Constant Heat Flux," International Journal of Heat and Mass Transfer, **50**(9-10) pp. 1938-1952.

[4] Chen, B., Wang, X., Zeng, R., 2008, "An Experimental Study of Convective Heat Transfer with Microencapsulated Phase Change Material Suspension: Laminar Flow in a Circular Tube Under Constant Heat Flux," Experimental Thermal and Fluid Science, **32**(8) pp. 1638-1646.

[5] Zeng, R., Wang, X., Chen, B., 2009, "Heat Transfer Characteristics of Microencapsulated Phase Change Material Slurry in Laminar Flow Under Constant Heat Flux," Applied Energy, **86**(12) pp. 2661-2670.

[6] Taherian, H., and Alvarado, J. L., 2010, "System Analysis of MPCM slurry Enhanced with Carbon Nanotubes as Heat Transfer Fluid," 2010 ASHRAE Annual Conference, June 26, 2010 - June 30, Anonymous Amer. Soc. Heating, Ref. Air-Conditoning Eng. Inc, Albuquerque, NM, United states, **116,** pp. 578-584

[7] Nakagawa, S., Hashimoto, T., Hayashi, T., 2010, "Fundamental Study on Heat Transfer Characteristics of Microencapsulated Phase Change Material Suspensions

Flowing in Circular Mini-pipe," 2010 12th IEEE Intersociety Conference on Thermal and Thermomechanical Phenomena in Electronic Systems, ITherm 2010, June 2, 2010 - June 5, Anonymous IEEE Computer Society, Las Vegas, NV, United states.

[8] Mulligan, J. C., D. P. Colvin, and Y. G. Bryant. "Microencapsulated phase-change material suspensions for heat transfer in spacecraft thermal systems." Journal of Spacecraft and Rockets **33**(2) (1996): 278-284.

[9] Seban, R. A., and McLaughlin, E. F., 1963, "Heat Transfer in Tube Coils with Laminar and Turbulent Flow," International Journal of Heat and Mass Transfer, **6**(5) pp. 387-395.

[10] Dravid, A. N., Smith, K. A., Merrill, E. W., 1971, "Effect of Secondary Fluid Motion on Laminar Flow Heat Transfer in Helically Coiled Tubes," AICHE Journal, **17**(5) pp. 1114-1122.

[11] Kalb, C. E., and Seader, J. D., 1974, "Fully Developed Viscous-flow Heat Transfer in Curved Circular Tubes with Uniform Wall Temperature," AICHE Journal, **20**(2) pp. 340-346.

[12] Janssen, L. A. M., and Hoogendoorn, C. J., 1978, "Laminar Convective Heat Transfer in Helical Coiled Tubes," International Journal of Heat and Mass Transfer, **21**(9) pp. 1197-1206.

[13] Manlapaz, R. L., and Churchill, S. W., 1981, "Fully Developed Laminar Convection from a Helical Coil," Chemical Engineering Communications, **9**(1-6) pp. 185-200.

[14] Prasad, B. V. S. S. S., Das, D. H., and Prabhakar, A. K., 1989, "Pressure Drop, Heat Transfer and Performance of a Helically Coiled Tubular Exchanger," Heat Recovery Systems & CHP, **9**(3) pp. 249-256.

[15] Ito, H., 1958, "Friction Factors for Turbulent Flow in Curved Pipes," ASME Meeting, Anonymous American Society of Mechanical Engineers (ASME), New York, NY, United States, pp. 9.

[16] Rennie, T. J., and Raghavan, V. G. S., 2005, "Experimental Studies of a Double-Pipe Helical Heat Exchanger," Experimental Thermal and Fluid Science, **29**(8) pp. 919-924.

[17] Fernandez-Seara, J., Uhia, F. J., Sieres, J., 2007, "A General Review of the Wilson Plot Method and its Modifications to Determine Convection Coefficients in Heat Exchange Devices," Applied Thermal Engineering, **27**(17-18) pp. 2745-2757.

[18] Kumar, V., Saini, S., Sharma, M., 2006, "Pressure Drop and Heat Transfer Study in Tube-in-Tube Helical Heat Exchanger," Chemical Engineering Science, **61**(13) pp. 4403-4416.

[19] Naphon, P., 2007, "Thermal Performance and Pressure Drop of the Helical-Coil Heat Exchangers with and without Helically Crimped Fins," International Communications in Heat and Mass Transfer, **34**(3) pp. 321-330.

[20] Incropera F P, Lavine A S, DeWitt D P. Fundamentals of heat and mass transfer[M]. John Wiley & Sons, 2011.

APPENDIX A

EES code

```
"Given variables"

$ifnot Parametrictable


$endif
Fluid$ = 'WATER'

"properties of  heat exchanger"

"this part is to calculate the hydraulic diameter"
do_core=0.963[in]*convert(in,m)          "Outer diameter of the core side--measured"
s_t_1=0.044[in]*convert(in,m)            "Wall thickness of the core side-measured"
di_core=do_core-2*s_t_1                  "Inner diameter of core side-
calculated"
do_shell=1.5[in]*convert(in,m)           "Outer diameter of the shell side--
measured"
di_shell=do_shell-2*s_t_1                "Inner diameter of the shell side-
calculated"
"Assume the thicknesses are the same for core side and shell side"

D_hd_h=(do_core+di_core)/2               "Hydraulic diameter of core side,know
as hot side,use average value"
D_hd_c=(do_shell+di_shell)/2-D_hd_h      "Hydraulic diameter of shell side,know
as cold side,use average value"

"this part is to calculate the mean velocity of the fluid pass through the HX"
Aih=pi*(di_core/2)^2                     "inner side area of the  HX hot
side,known as core side"
Aic=pi*(((di_shell+do_shell)/2)/2)^2-pi*(D_hd_h/2)^2    "inner side area of the  HX
cold side,know as shell side"

"Properties of cold fluid"
Tm_c=((T2ci+T2co)/2)                     " Mean temperature (Tm_c) "
rho_c=Density(Fluid$,T=Tm_c,P=Po#)       "Density (rho_c)"
cp_c=SpecHeat(Fluid$,T=Tm_c,P=Po#)       "Specific heat (cp_c)"
k_c=Conductivity(Fluid$,T=Tm_c,P=Po#)    "Thermal conductivity (k_c)"
Pr_c=Prandtl(Fluid$,T=Tm_c,P=Po#)        "Prandtl number (Pr_c)"
```

```
mu_c=Viscosity(Fluid$,T=Tm_c,P=Po#)          "Viscosity (mu_c)"

"Properties of hot fluid"
Tm_h=(T2hi+T2ho)/2                           "Mean temperature (Tm_h) "
rho_h=947[kg/m^3]                            "Density (rho_h),measured"
cp_h=Q_c/(DT_h*m_dot_h)                      "Specific heat (cp_h)"
mu_h=0.00166 [pa*s]                          "Viscosity (mu_h)"

"Hot fluid calculations"
m_dot_h=V_fl_h*convert(l/min,m^3/s)*rho_h    "Mass flow rate of hot fluid "
C_h=m_dot_h*cp_h                             "Heat capacity of hot fluid"
DT_h=abs(T2hi-T2ho)                          "Temp difference of hot fluid "
Q_h=C_h*DT_h                                 "Heat rate of hot fluid"
V_vh=V_fl_h*convert(l/min,m^3/s)/Aih         "mean velocity of hot fluid"

"Cold fluid calculations"
m_dot_c=V_fl_c*convert(l/min,m^3/s)*rho_c    "Mass flow rate of cold fluid"
C_c=m_dot_c*cp_c                             "Heat capacity of cold fluid"
DT_c=T2co-T2ci                               "Temp difference of cold fluid"
Q_c= C_c*DT_c                                "Heat rate of cold fluid"
V_vc=V_fl_c*convert(l/min,m^3/s)/Aic         "mean velocity of cold fluid"

"Heat exchanger calculations"
dT_1=abs(T2hi-T2co)                          " Log mean temperature difference
(LMTD)"
dT_2=T2ho-T2ci
dT_lm=(dT_2-dT_1)/ln(dT_2/dT_1 )



C_min=min(C_c, C_h)
C_max=max(C_c, C_h)
C_r=C_min/C_max                              "Heat capacity ratio"

UA=Q_c/dt_lm                                 "NTU calculation"
NTU=UA/C_min

Q=C_c*(T2ci-T2co)                            "heat exchanger effctiveness"
Q_max=C_min*(T2hi-T2ci)
epsilon_hx=abs(Q/Q_max)

Re_h=rho_h*V_vh*D_hd_h/mu_h          "Reynolds Number-core side,known as
hot side"
```

```
Re_c=rho_c*V_vc*D_hd_c/mu_c                "Reynolds Number-shell side,known as cold side"

Dm=14.5[in]*convert(in,m)                  "Diameter of the coil--From manufactuter"
De_h=Re_h*(do_core/Dm)^(1/2)               "Dean number--core side,known as hot side"
De_c=Re_c*((do_shell-do_core)/Dm)^(1/2)     "Dean number--shell side,known as cold side"

"overall heat transfer coefficient"
U=Q_h/(A_s*dt_lm)                          "overall heat transfer coefficient "
A_s=pi*(d_hd_h)*L_hx_core                  "overall heat transfer surface area, use hydraulic diameter of core side as real diameter"

"friction factor"
Vol_hx_core=1.8*10^(-3)
L_hx_core=Vol_hx_core/Aih
f=(2*D_hd_h*delta_P_hx*convert(psi,pa))/(rho_h*L_hx_core*V_vh^2)

DP_sys_kpa=delta_P*convert(psi,kpa)
Delta_P_hx_kpa=delta_P_hx*convert(psi,kpa)

"Percentage of Particles Under Phase Change (phi_MPCM)" "**CHECK**"
abs(Q)=m_dot_h*DT_h*((1-
MF_MPCM)*cp_carrier+MF_MPCM*cp_MPCM)+phi_MPCM*(m_dot_h*MF_MPC
M*lambda_MPCM)
cp_carrier=SpecHeat(Fluid$,T=Tm_h,P=Po#)    "Specific heat of the carrier fluid"
MF_MPCM=0.046
lambda_MPCM=152[kj/kg]
cp_MPCM=2[kj/kg-c]
```

APPENDIX B

Uncertainty analysis

Uncertainty analysis of the experimental measurements was carried out using the Engineering Equation Solver (EES) software. The measured data which contained quantifiable uncertainties were as follows: the temperature readings of the thermocouples, the pressure drop of the HX coil side, the mass flowrate of the coil side, and the readings of the viscometer. The EES software follows the multivariate propagation of error formula as seen in Equation (35). The uncertainties of these measured variables can be seen in Table 9.

If $U = U(X_1, X_2, \dots, X_n)$ with uncertainties $\sigma_1, \sigma_2, \dots, \sigma_n$, then (35)

$$\sigma_U = \sqrt{\left(\frac{\partial U}{\partial X_1}\right)^2 {\sigma_{X_1}}^2 + \left(\frac{\partial U}{\partial X_2}\right)^2 {\sigma_{X_2}}^2 + \cdots + \left(\frac{\partial U}{\partial X_n}\right)^2 {\sigma_{X_n}}^2}$$

Table 9 Measured variables and uncertainties

Parameter	Uncertainty
ΔP	±0.04 %
T	±0.1 ℃
$\dot{m}_h$	±0.5%
Viscostiy	±1%

Uncertainties were calculated for the composite coil PEC, effectiveness, and NTU for both tests using water and MPCM slurry as HTF. The calculated data and their uncertainties during the tests can be seen in Table 10, 11 and 12.

Table 10 Calculated data uncertainties during tests using water as HTF in the coils and water in the shell

Test Number	**Effectiveness, ε**	**NTU**
1	0.6101 ± 0.0083 (±1.39%)	1.68 ± 0.01515 (±0.94%)
2	0.618 ±0.01024 (±1.72%)	1.71 ± 0.01963 (±1.16%)
3	0.6136 ± 0.007536 (±1.23%)	1.72 ± 0.01891 (±1.09%)
4	0.618 ± 0.007017 (±1.14%)	1.741 ± 0.02123 (±1.23%)
5	0.625 ± 0.008816 (±1.42%)	1.752 ± 0.02069 (±1.18%)
6	0.6292 ± 0.01011 (±1.61%)	1.783 ± 0.02138 (±1.22%)
7	0.633 ± 0.010429 (±1.65%)	1.77 ± 0.02274 (±1.26%)

Table 11 Calculated data and uncertainties during tests using 4.6% MPCM slurry as HTF in the coils and water in the shell

Test Number	PEC	Effectiveness, ε	NTU
1	1.048 ± 0.0157 (±1.52%)	0.7093 ± 0.008313 (±1.18%)	2.052 ± 0.02259 (±1.10%)
2	1.070 ± 0.0127 (±1.25%)	0.7093 ± 0.007365 (±1.04%)	2.084 ± 0.02187 (±1.05%)
3	1.066 ± 0.0131 (±1.15%)	0.7126 ± 0.01046 (±1.49%)	2.086 ± 0.02991 (±1.43%)
4	1.094 ± 0.0149 (±1.39%)	0.7209 ± 0.00976 (±1.35%)	2.16 ± 0.02731 (±1.27%)
5	1.050 ± 0.0137 (±1.31%)	0.7241 ± 0.008614 (±1.19%)	2.161 ± 0.03088 (±1.43%)
6	1.056 ± 0.0141 (±1.36%)	0.7222 ± 0.009167 (±1.27%)	2.187 ± 0.03142 (±1.44%)
7	1.157 ± 0.0106 (±0.94%)	0.7203 ± 0.01024 (±1.46%)	2.264 ± 0.02867 (±1.27%)

Table 12 Calculated data and uncertainties during tests using 4.6% MPCM slurry as HTF in the coils and water in the shell

Test Number	PEC	Effectiveness, ε	NTU
1	0.956 ±0.01059 (±1.11%)	0.7391 ±0.008379 (±1.13%)	2.232 ±0.02155 (±0.97%)
2	1.010 ±0.01339 (±1.33%)	0.7444 ±0.009907 (±1.33%)	2.309 ±0.02268 (±0.99%)
3	0.988 ±0.0145 (±1.49%)	0.7419 ±0.01058 (±1.43%)	2.331 ±0.02451 (±1.05%)
4	0.995 ±0.01567 (±1.58%)	0.75 ±0.009516 (±1.27%)	2.343 ±0.02675 (±1.14%)
5	0.981 ±0.01338 (±1.37%)	0.7582 ±0.008149 (±1.07%)	2.391 ±0.02240 (±0.94%)
6	0.967 ±0.01587 (±1.64%)	0.7553 ±0.009175 (±1.22%)	2.411 ±0.02647 (±1.10%)
7	1.037 ±0.01597 (±1.55%)	0.7634 ±0.001009 (±1.33%)	2.461 ±0.02964 (±1.21%)